The Influence of Calcium Chloride Deicing Salt on Phase Changes and Damage Development in Cementitious Materials

Yaghoob Farnam[1], Sarah Dick[2], Andrew Wiese[3], Jeffrey Davis[4], Dale Bentz[5], and Jason Weiss[6]

[1] Graduate Research Assistant, Lyles School of Civil Engineering, Purdue University, 550 Stadium Mall Dr., West Lafayette, IN 47907, USA, yfarnam@purdue.edu

[2] Undergraduate Research Assistant, Lyles School of Civil Engineering, Purdue University, 550 Stadium Mall Drive, West Lafayette, IN 47907, USA, dicks@purdue.edu

[3] Graduate Research Assistant, Lyles School of Civil Engineering, Purdue University, 550 Stadium Mall Dr., West Lafayette, IN 47907, USA, awiese@purdue.edu

[4] Materials Research Engineer, Materials Measurement Science Division, National Institute of Standards and Technology, 100 Bureau Drive, Stop 8615, Gaithersburg, MD 20899, USA, jeff.davis@nist.gov

[5] Chemical Engineer, Materials and Structural Systems Division, National Institute of Standards and Technology, 100 Bureau Drive, Stop 8615, Gaithersburg, MD 20899, USA, dale.bentz@nist.gov

[6] Jack and Kay Hockema Professor of Civil Engineering, Director of Pankow Materials Laboratory, Lyles School of Civil Engineering, Purdue University, 550 Stadium Mall Dr., West Lafayette, IN 47907, wjweiss@purdue.edu

ABSTRACT

The conventional $CaCl_2$-H_2O phase diagram is often used to describe how calcium chloride behaves when it is used on a concrete pavement undergoing freeze-thaw damage. However, the chemistry of the concrete can alter the appropriateness of using the $CaCl_2$-H_2O phase diagram. This study shows that the $Ca(OH)_2$ present in a hydrated portland cement can interact with $CaCl_2$ solution creating a behavior that is similar to that observed in isoplethal sections of a ternary phase diagram for a $Ca(OH)_2$-$CaCl_2$-H_2O system. As such, it is suggested that such isoplethal sections provide a reasonable model that can be used to describe the behavior of concrete exposed to $CaCl_2$ solution as the temperature changes. Specifically, the $Ca(OH)_2$ can react with $CaCl_2$ and H_2O resulting in the formation of calcium oxychloride. The formation of the calcium oxychloride is expansive and can produce damage in concrete at temperatures above freezing. Its formation can also cause a significant decrease in fluid ingress into concrete. For solutions with $CaCl_2$ concentrations greater than about 11.3 % (by mass), it is found that calcium oxychloride forms rapidly and is stable at room temperature (23 °C).

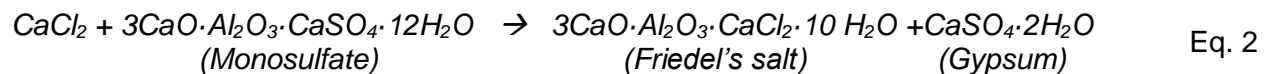Keywords: Calcium Oxychloride, Concrete, Deicing Salt, Freeze-Thaw, Damage, Phase Change.
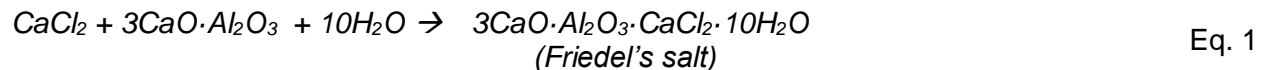
1.0 Introduction

Concrete pavement and flatwork may degrade when they are exposed to deicing chemicals. The deicing salt solution can be absorbed into the pores of concrete and can alter the cementitious matrix. The interaction between the deicing salt solution and the cementitious matrix may result in damage to the concrete [1]. Physical damage can occur due to a number of processes: 1) exposure of concrete with a high degree of saturation to freeze-thaw cycles [2–7], 2) scaling of concrete surfaces [8–11], 3) crystallization of salt in concrete pores that results in production of an internal stress [12–14], and 4) expansive forces as a result of corrosion of reinforcement when a chloride-based deicing salt is used [15,16]. While the physical attack of deicing salts has been widely investigated, the chemical reaction between the matrix and the deicing salts has been studied less frequently.

The use of deicing salts can cause damage in cementitious materials even if a concrete does not experience freezing and melting [10,17–22]. This may be caused by the formation of Friedel's salt, Kuzel's salts [18,21–23], and/or calcium oxychloride, changes in the pore solution properties [4,17], or changes in the microstructure of hydration products [19,20,22]. Deicing salt solution, like many external solutions, may also dissolve calcium hydroxide, causing leaching that leads to an increase in permeability and a reduction of concrete alkalinity [16,24].

Deicing salts have different chemical and physical interactions with cementitious materials. The use of NaCl deicing salt increases freeze-thaw damage in concrete. This increase in freeze-thaw damage has been explained by the formation of an unexpected phases and the creation of osmotic pressures [4,17,20]. Concrete exposed to $CaCl_2$ and $MgCl_2$ de-icing salts also exhibited changes in the concrete microstructure. These changes have been accompanied by a severe cracking and deterioration, even if the concrete did not experience any freeze-thaw cycles [18,21,22,25].

Chloride-based deicers can result in the formation of calcium chloroaluminate phases such as Friedel's salt and Kuzel's salt that can bind chloride [22,23,26–28]. Possible reactions for the formation of Friedel's salt in the presence of $CaCl_2$, for example, are shown in Eq. 1 [28] and Eq. 2 Kuzel's salt ($3CaO \cdot Al_2O_3 \cdot 0.5CaSO_4 \cdot 0.5CaCl_2 \cdot 11H_2O$) may be also produced in the presence of chloride-based deicing salts [23,29].

$$CaCl_2 + 3CaO \cdot Al_2O_3 + 10H_2O \rightarrow 3CaO \cdot Al_2O_3 \cdot CaCl_2 \cdot 10H_2O$$
$$(Friedel's\ salt)$$
Eq. 1

$$CaCl_2 + 3CaO \cdot Al_2O_3 \cdot CaSO_4 \cdot 12H_2O \rightarrow 3CaO \cdot Al_2O_3 \cdot CaCl_2 \cdot 10\ H_2O + CaSO_4 \cdot 2H_2O$$
$$(Monosulfate) \qquad (Friedel's\ salt) \qquad (Gypsum)$$
Eq. 2

Collepardi et al. [19] concluded that $CaCl_2$ can result in a reaction that leads to damage, even in the absence of freeze-thaw cycles. The chemical reaction is described by the formation of calcium oxychloride (Eq. 3).

$$3Ca(OH)_2 + CaCl_2 + 12H_2O \rightarrow CaCl_2 \cdot 3Ca(OH)_2 \cdot 12H_2O \qquad (Calcium\ oxychloride)$$
Eq. 3
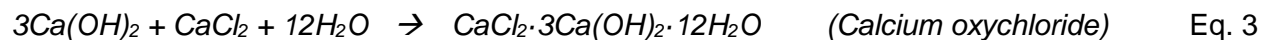
The temperature at which calcium oxychloride forms is above the freezing point of water [18,21,22,26,30,31]. The reaction has also been described as a rapid reaction between calcium hydroxide and calcium chloride, however the rate of this reaction has not been quantified. The reaction between calcium chloride and calcium hydroxide (i.e., solid phases in the reaction) is expansive and can be destructive when it forms in the concrete matrix due to the internal

2

hydraulic pressures that may be generated. Calcium oxychloride is unstable at room temperature and lower levels of relative humidity [18,32]. Calcium oxychloride has been reported with different molar ratios (i.e., $CaCl_2 \cdot 3Ca(OH)_2 \cdot 12H_2O$, $CaCl_2 \cdot Ca(OH)_2 \cdot xH_2O$, and $CaCl_2 \cdot Ca(OH)_2$); these phases may coexist and be interchangeable in $Ca(OH)_2$-$CaCl_2$-H_2O systems. However, $CaCl_2 \cdot 3Ca(OH)_2 \cdot 12H_2O$ was observed to be destructive and can be simply altered to $CaCl_2 \cdot Ca(OH)_2$ or $CaCl_2 \cdot Ca(OH)_2 \cdot xH_2O$ if the ambient temperature or humidity varies [32–34].

Figure 1a shows the conventional phase diagram for the $CaCl_2$-H_2O binary system. Figure 1b illustrates an isoplethal section from the work of Vol'nov and Latysheva, and Makarov and Vol'nov [35,36] for a ternary system containing $Ca(OH)_2$-$CaCl_2$-H_2O. It should be mentioned that the formation of the different phases in this isoplethal section (Figure 1b) were reported only as a function of temperature and $CaCl_2$ concentration. As such, the effect of $Ca(OH)_2$:$CaCl_2$ mass/molar ratio on the formation of the different phases was not considered, but is important. Different phases exist in the $Ca(OH)_2$-$CaCl_2$-H_2O system: $CaCl_2$ solution, $Ca(OH)_2$, ice, $CaCl_2 \cdot 3Ca(OH)_2 \cdot 12H_2O$, $CaCl_2 \cdot Ca(OH)_2 \cdot xH_2O$, and $CaCl_2 \cdot nH_2O$ (where n is 2, 4, or 6).
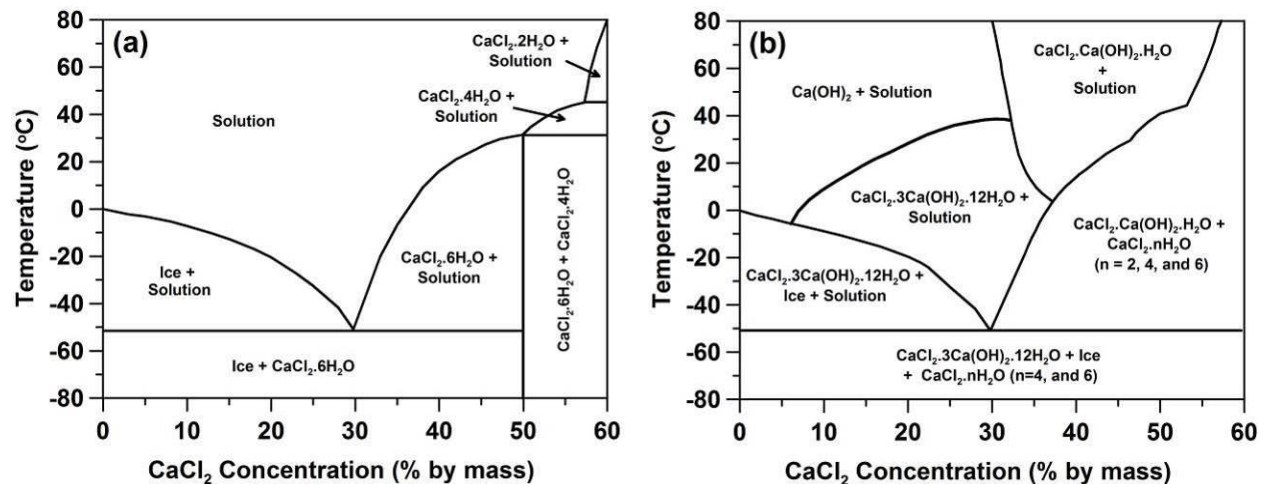

Figure 1 – a) Classical phase diagram for $CaCl_2$-H_2O system and b) an isoplethal section for a $Ca(OH)_2$-$CaCl_2$-H_2O system developed from [35,36] ($Ca(OH)_2$:$CaCl_2$ molar ratios <= 0.5).

A conventional interpretation of the $CaCl_2$-H_2O phase diagram (Figure 1a) shows that using a higher concentration of $CaCl_2$ can reduce freezing temperature. However, Figure 1b shows the $Ca(OH)_2$-$CaCl_2$-H_2O isoplethal section that occurs when $Ca(OH)_2$ is added as a third phase. It can be seen that $Ca(OH)_2$ from the cementitious matrix in concrete alters the behavior. The interaction between $Ca(OH)_2$ and $CaCl_2$ can alter concrete microstructure and pore solution properties resulting in the formation of calcium oxychloride. The formation and precipitation of calcium oxychloride (as an expansive phase) may change transport properties of concrete due to pore blocking and may also cause a severe deterioration due to internal expansion, even when the concrete temperature remains above 0 °C, since it forms at a temperature greater than 0 °C (Figure 1b).

The temperature at which calcium oxychloride forms, its relation to the concentration of $CaCl_2$ solution, and its rate of formation can play an important role in concrete freeze-thaw behavior, concrete degradation, and fluid ingress into concrete.

The main purpose of this study is to provide an improved understanding of the interaction between the calcium chloride deicing salt and cementitious material and to investigate its impact

on concrete deterioration. In this paper, several techniques were used to understand the $Ca(OH)_2$-$CaCl_2$-H_2O system and isoplethal sections (varying the concentration of $Ca(OH)_2$) were used as a model system for a cementitious system. The temperatures at which different phase changes occur were also determined.

2.0 Experimental Program

Mortar freeze-thaw behavior, mortar degradation, and fluid ingress into mortar were evaluated when the specimens were exposed to a $CaCl_2$ deicing salt. First, a low temperature longitudinal guarded comparative calorimeter equipped with acoustic emission detection (AE-LGCC) was used to investigate the damage (cracking) that occurs during the freezing and melting of mortar specimens saturated with solutions containing different concentrations of $CaCl_2$. Micro focused X-ray fluorescence (μXRF) examination was used to study the $CaCl_2$ solution ingress into these mortar specimens. Low temperature differential scanning calorimetry (LT-DSC) was used to determine phase changes (associated with solution, ice, eutectic solid, and calcium oxychloride) which can exist in the hydrated cement paste exposed to $CaCl_2$ solutions. Finally, isothermal micro-calorimetry (IMC) at 23 °C was used to determine the onset, rate, and heat of reaction when a hydrated cement powder is in contact with a $CaCl_2$ solution. Table 1 summarizes the experimental program that was carried out in this study.

Table 1 - Experimental program

Experiment	Sample Type	CaCl₂ solution concentration (% by mass of solution)	Purpose
AE-LGCC	Mortar	0, 0.96, 3, 5, 8, 10, 13, 15, 20, 25, and 29.8	Freeze-thaw damage development
XRF	Mortar	0, 5, 10, 15, 20, 25, and 29.8	CaCl₂ solution ingress and chloride profile
LT-DSC	Series I- CaCl₂ solution Series II- Pore solution Series III- Ca(OH)₂ powder with Ca(OH)₂:CaCl₂ molar ratio greater than 3 Series IV- Ca(OH)₂ powder with Ca(OH)₂:CaCl₂ molar ratio equal to or less than 3 Series V- Hydrated cement powder	Series I- 0, 3, 5, 8, 10, 13, 15, 18, 20, 23, 25, 28, 29.8, and 35 Series II- 0, 5, 10, 15, 20, 25, 29.8, and 35 Series III- 0, 5, 10, 15, 20, and 25 Series IV- 0, 5, 10, 15, 20, and 25 Series V- 0, 5, 10, 15, 20, 25, 29.8, and 33	Development of phase diagram for: • Concrete pore solution and CaCl₂ • Ca(OH)₂-CaCl₂-H₂O • Hydrated cement powder and CaCl₂
IMC	Series I: Ca(OH)₂ powder Series II: Hydrated cement powder	Series I- 0, 5, 10, 15, 20, and 25 Series II- 0, 5, 10, 15, 20, 25, and 29.8	Determination of calcium oxychloride formation rate

2.1 Materials

Type I ordinary portland cement (OPC) was used in this study. This cement had a calculated Bogue phase composition of 60 % tricalcium silicate (C_3S), 10 % dicalcium silicate (C_2S), 9 % tricalcium aluminate (C_3A), and 10 % tetracalcium aluminoferrite (C_4AF) by mass, and a reported Blaine fineness of 375 m^2/kg. The total equivalent alkali was 0.86 %, originating from 0.35 % of Na_2O and 0.77 % of K_2O, by mass. Aggregates used to prepare mortar specimens consisted of natural sand with a maximum size of 4.75 mm, specific gravity of 2.61, fineness modulus of 2.89, and a water absorption value of 2.2 % by mass.

Granular reagent calcium chloride dihydrate with a formula weight of 147.010 g/mol and de-ionized (DI) water were used to prepare $CaCl_2$ solutions. Calcium hydroxide (CH) powder used in this study had a $Ca(OH)_2$ purity greater than 98.2 % and a formula weight of 74.09 g/mol. Potassium hydroxide pellets (assay (KOH) >= 86 %) and sodium hydroxide pellets (assay

(NaOH) >= 98 %) were also used with formula weights of 56.110 g/mol and 40.000 g/mol, respectively.

2.2 Mixture Proportioning, Specimen Preparation, and Conditioning

2.2.1 Mortar Specimens

Mortar specimens were prepared for use in freeze-thaw testing and XRF examination. A mixture with a sand volume fraction of 55 % and a water-to-cement ratio (*w/c*) of 0.42 by mass was prepared. No chemical admixtures or supplementary cementitious materials were used. The mass of cement, water, and sand (in saturated-surface-dry (SSD) condition) were 612 kg, 257 kg, and 1435 kg per m^3 of total material volume, respectively. Specimens were prepared in a standard mortar mixer in accordance with ASTM C305-12 [37]. The entrapped air content in mortar samples was obtained to be 4.5 % by volume (standard deviation = 0.3 %) using a concrete air meter. The mortar was cast in 25.4 mm × 25.4 mm × 300 mm (1 in × 1 in × 11.81 in) molds and the samples were demolded after 24 h. All mortar bars were then sealed in double plastic bags and cured for 28 d in these sealed conditions at 23 °C ± 0.5 °C. After 28 d of curing, the mortar bars were cut using a wet saw to 25.4 mm × 25.4 mm × 50.8 mm (1 in × 1 in × 2 in) specimens. These specimens were then placed in a vacuum oven at 65 °C ± 1 °C and a pressure of 20 mm Hg ± 5 mm Hg for 7 d. The ± 1 °C and ± 5 mm Hg are indicative of the nominal operating range encountered when running the experiment. Two cement paste specimens were also prepared, cured, and dried in a manner similar to that employed for the mortar specimens, to monitor the degree of hydration and to determine the density of the cement paste. The average degree of hydration was determined to be 77.9 % (standard deviation = 2 %) by obtaining the non-evaporable water content as the relative mass loss between 105 °C and 1100 °C, corrected for the loss-on-ignition of the initial dry cement powder.

To saturate the specimens with $CaCl_2$ solution, the specimens that were dried in the vacuum oven were placed in a desiccator using two small spacers underneath each specimen to provide a small gap between the bottom of the container and the lower surface of specimen. The specimens were evacuated to a pressure of 10 mm Hg ± 5 mm Hg for 3.5 h. After evacuation and while still under vacuum, de-aerated $CaCl_2$ solution (de-aerated by vacuuming the solution for 15 min) was introduced into the desiccator to cover the specimens for 1 h. Soaked specimens submerged in a $CaCl_2$ solution were transferred to a 23 °C ± 0.5 °C chamber before testing, where they were kept in a beaker for 3 d (covered to prevent evaporation). This condition was considered to be fully saturated (i.e., assumed 100 % degree of saturation). The porosity, SSD density, and oven-dry (OD) density of mortar specimens were estimated to be 20.6 % by volume, 2267 kg/m^3, and 2077 kg/m^3, respectively, according to ASTM C642-13 [38]. The porosity, SSD density, and oven-dry (OD) density of cement paste were also estimated to be 35.8 % by volume (standard deviation = 0.5 %), 1931 kg/m^3 (standard deviation = 13.2 kg/m^3), and 1574 kg/m^3 (standard deviation = 18.2 kg/m^3), respectively, according to ASTM C642-13 [38].

2.2.2 Solution Preparation

Granular dihydrate calcium chloride (75.49 % $CaCl_2$ and 24.51 % DI water) and DI water were mixed to prepare $CaCl_2$ solutions. A wide range of $CaCl_2$ concentration between 0 % and 35 % by mass of solution was used. KOH and NaOH were used to make a synthetic pore solution with [K+], [Na+], and [OH-] of 0.65 mol/L, 0.45 mol/L, and 1.10 mol/L, respectively. This was calculated using software for estimation of pore solution properties developed previously (http://concrete.nist.gov/poresolncalc.html) [39] for the cement used in this study (considering a 100 % degree of hydration in a sealed condition). Different percentages of $CaCl_2$ salt were

added to the pore solution with respect to the corresponding mass of DI water in the pore solution to achieve the desired percent $CaCl_2$ by mass of solution.

2.2.3 Powder Specimens

Powder specimens were blended with solutions described in Section 2.2.2 and used for LT-DSC and IMC experiments. To prepare hydrated cement powder, cement paste was prepared using a vacuum mixer with a capacity of 500 ml and a speed of 400 rpm. Cement paste w/c was once again 0.42 by mass. The cement paste was then cast in plastic containers and cured for one year in a sealed condition. The average degree of hydration for this cement paste was determined to be 90.4 % by obtaining the non-evaporable water content as the relative mass loss between 105 °C and 1100 °C, corrected for the loss-on-ignition of the initial dry cement powder. After one year, the cement paste specimens were ground in a mortar and pestle and a 75-µm (No. 200) sieve was used to separate larger particles. The hydrated cement powder was stored in a vacuum oven at 65 °C ± 1 °C and a pressure of 20 mm Hg ± 5 mm Hg for 3 d to remove moisture. To investigate the reaction between portlandite and $CaCl_2$ solution occurring in concrete, calcium hydroxide powder was used. For these specimens, the $CaCl_2$ solutions were mixed with the $Ca(OH)_2$ powder just before testing.

2.3 Testing Procedure
2.3.1 Freeze-Thaw Experiment

An Acoustic Emission Low Temperature Longitudinal Guarded Comparative Calorimeter (AE-LGCC) was used to perform the freeze-thaw experiments [4]. A temperature gradient was established in the test specimen to produce a one-dimensional heat flow. Heat losses in the lateral direction were minimized by using a longitudinal guard and thermal insulation. Two meter bars with known thermal properties were used on the top and bottom of the mortar specimens, to calculate the heat flow through the specimens. To quantify damage and cracking in the specimens, acoustic emission (AE) monitoring was used. One broadband acoustic sensor was attached to the specimen to record acoustic activity during the freeze-thaw test. In addition, wave speed (pulse velocity) was measured on all specimens using a pulsed wave generated by two coupled AE sensors and passing through the length of the specimen, before and after the freeze-thaw test. These AE-LGCC testing protocols have been previously described [4,17,40]. Acoustic emission testing has shown promising performance for assessing the damage development in cementitious materials [17,41,42].

Mortar specimens were saturated with a solution of DI water and $CaCl_2$ (0.96 %, 3 %, 5 %, 8 %, 10 %, 13 %, 15 %, 20 %, 25 %, and 29.8 % $CaCl_2$ by mass). For each concentration, one specimen was prepared. Uncertainty in this experiment was estimated using one additional specimen with 0 % $CaCl_2$ (DI water).

The temperature of mortar specimens was varied from 24 °C to -40 °C by using a cold plate. The initial temperature of the test was set to remain at 24 °C for one hour to allow the specimen to equilibrate. After the initial temperature became stable, the bottom surface was cooled at a rate of 2 °C/h within 32 h. At -40 °C, the temperature was kept constant for 4 h to allow the specimen to again reach equilibrium. Then, the temperature was increased to 24 °C at a rate of 4 °C/h within 16 h. The test was complete after one cycle.

2.3.2 X-Ray Fluorescence (XRF)

An Eagle III (EDAX) micro X-ray fluorescence system was used to estimate the penetration depth of chloride ions into the specimens through the use of hyperspectral X-ray imaging. Imaging was accomplished by stepping the stage and addressing a focused X-ray beam to an array of equally spaced points. At each point, a full X-ray spectrum is collected and the

elements of interest (chlorine in this study) were integrated over their respective spectral ranges. The resultant images show areas of high and low chloride concentration across the full specimen, as well as the gradient of concentration from the interior to the exterior of the mortar specimen. This imaging technique is described in [43]. Seven mortar specimens were imaged. The mortar specimens were previously saturated with 0 %, 5 %, 10 %, 15 %, 20 %, 25 %, and 29.8 % (by mass) $CaCl_2$ solutions. They were then broken exposing a cross section of the surface for µXRF imaging.

2.3.3   Low Temperature Differential Scanning Calorimetry (LT-DSC)

A LT-DSC instrument was used with an operating range of -90 °C to 550 °C to study low temperature phase transitions. The heat flow associated with phase transitions in materials was obtained. High volume stainless steel hermetic pans were used. The initial temperature of the test was set to equilibrate at 25 °C. After the initial temperature became stable, the LT-DSC cell was cooled to -90 °C with a cooling rate of 5 °C/min. The specimen temperature was kept constant at this temperature (-90 °C) for one min to allow the specimen to equilibrate. A cycle of heating and cooling was established between -90 °C and 70 °C. The specimen equilibrated again at -90 °C for 5 min; and the temperature of the specimen was increased to 70 °C at a rate of 5 °C/min.

Five different systems were studied. In the first series, DI water-$CaCl_2$ solutions were tested. In the second series, pore solutions and $CaCl_2$ were tested. For the first and second series, a total solution mass of 3 mg to 5 mg was used in LT-DSC. In the third series, calcium hydroxide powder was mixed with different salt solutions with a mass ratio of 1:1 (equivalent to a $Ca(OH)_2$:$CaCl_2$ molar ratio greater than 3). A 9 mg to 11 mg powder sample was mixed with 9 mg to 11 mg of solution, and they were tested in the LT-DSC immediately after mixing (0 d), 1 d after mixing, and 7 d after mixing. In the fourth series, specimens with $Ca(OH)_2$:$CaCl_2$ molar ratios less than or equal to 3 (1:1 and 1:3) were prepared with different salt solutions; and they were tested in the LT-DSC immediately after mixing (0 d). This was done to investigate the effect of the $Ca(OH)_2$:$CaCl_2$ molar ratio on the formation temperature of calcium oxychloride, since different types of calcium oxychloride (i.e., $3Ca(OH)_2 \cdot CaCl_2 \cdot 12H_2O$, $Ca(OH)_2 \cdot CaCl_2 \cdot xH_2O$, and $Ca(OH)_2 \cdot CaCl_2$) can exist with different $Ca(OH)_2$:$CaCl_2$ molar ratios. It should be noted that mixing calcium hydroxide powder with the 29.8 % $CaCl_2$ solution could not be achieved, due to a very fast reaction and near immediate solidification. In the fifth series, cement paste powder was mixed with salt solutions with a 1:1 mass ratio; 9 mg to 11 mg of powder was mixed with 9 mg to 11 mg of solution and was tested at three different ages after mixing with $CaCl_2$ solution: immediately after mixing (0 d), 1 d after mixing, and 7 d after mixing.

2.3.4   Isothermal Micro-Calorimetry (IMC)

A TAM Air isothermal micro-calorimeter was used to measure the heat released during the reaction between cement paste powder or calcium hydroxide powder and $CaCl_2$ solution under constant temperature conditions (23 ºC ± 0.1 ºC). The heat release can be used to determine the rate of reaction. An internal 20 mL admix ampoule was used to determine the heat of reaction as soon as solution was introduced to the powder. The powder was first placed in a vial and sealed; and the attached syringes were filled with solution. Then, the admix ampoule was placed in the isothermal calorimetry cell until all the components become stable and equilibrated at 23 ºC ± 0.1 ºC. While detecting heat flow, the solution was gently injected to the vial after equilibration and mixed with the powder for 90 s by an established stirrer in the admix ampoule.

Two series of experiments were performed in the isothermal calorimeter. In the first series, 2 g of calcium hydroxide powder was mixed with 2 g of solution with different concentrations of $CaCl_2$ (0 %, 5 %, 10 %, 15 %, 20 %, and 25 % by mass). Two more tests with different powder

to solution mass ratio were also performed to study the $Ca(OH)_2$:$CaCl_2$ molar ratios (1:1 and 1:3). It should be noted that mixing calcium hydroxide powder with 29.8 % $CaCl_2$ solution was again unachievable due to a very fast reaction and very rapid solidification. In the second series, 2 g of cement paste powder was mixed with 2 g of solution with different concentrations of $CaCl_2$ (0 %, 5 %, 10 %, 15 %, 20 %, 25 %, and 29.8 % by mass).

3.0 Results and Discussion
3.1 Freeze-Thaw Temperature and Fluid Ingress in Mortar Samples (AE-LGCC Experiment)

Heat flow was monitored using the AE-LGCC unit; and phase changes were detected by using the heat flow curve and observing any exothermic/endothermic behaviors. Figure 2 shows temperature (at different locations of the specimen and the meter bars) as a function of time (the temperature of the specimen changed between +25 °C and –40 °C). During the rapid freezing that is observed in the experiment, an increase in the temperature (shown by an arrow in this figure) was observed due to the heat of fusion at the freezing point, consistent with ice formation. Melting occurs more gradually over a range of temperatures depending on the pore sizes present in the mortar, such that the specimen temperature only lags slightly behind the heating rate during this portion of the single freeze-thaw cycle due to the energy absorption from the surrounding environment during endothermic ice melting.

Heat flow inward/outward of the mortar specimen was calculated [4] and is shown in Figure 3 as a function of the specimen temperature. The freezing was identified as an exothermic peak during the specimen cooling; and the melting was observed as an endothermic peak. While the freezing peak was sharp, the melting peak occurred gradually. This is due to supercooling action [44] taking place during freezing.

The freezing and melting points detected by AE-LGCC are compared to the conventional $CaCl_2$-H_2O phase diagram in Figure 4. Supercooling can be seen during cooling since the freezing took place at a lower temperature than the liquidus line. As the solution concentration increases, a slight reduction in freezing and melting temperatures was observed in comparison with the $CaCl_2$ liquidus line. It should be mentioned that for higher concentrations, the freezing points were even above the liquidus line of conventional $CaCl_2$. This may be due to $CaCl_2$ consumption due to chemical reactions to form Friedel's salt, Kuzel's salt, or calcium oxychloride. In addition, no exothermic/endothermic behavior was observed associated with calcium oxychloride formation (which is expected to be above 0 °C, Figure 1b) in the temperature range applied in this experiment (24 °C to -40 °C). The reasons may include either: 1) the calcium oxychloride formed at a temperature higher than the temperature range applied by the AE-LGCC, or 2) the amount of heat released/absorbed during its phase change was relatively small and was not detected by AE-LGCC.
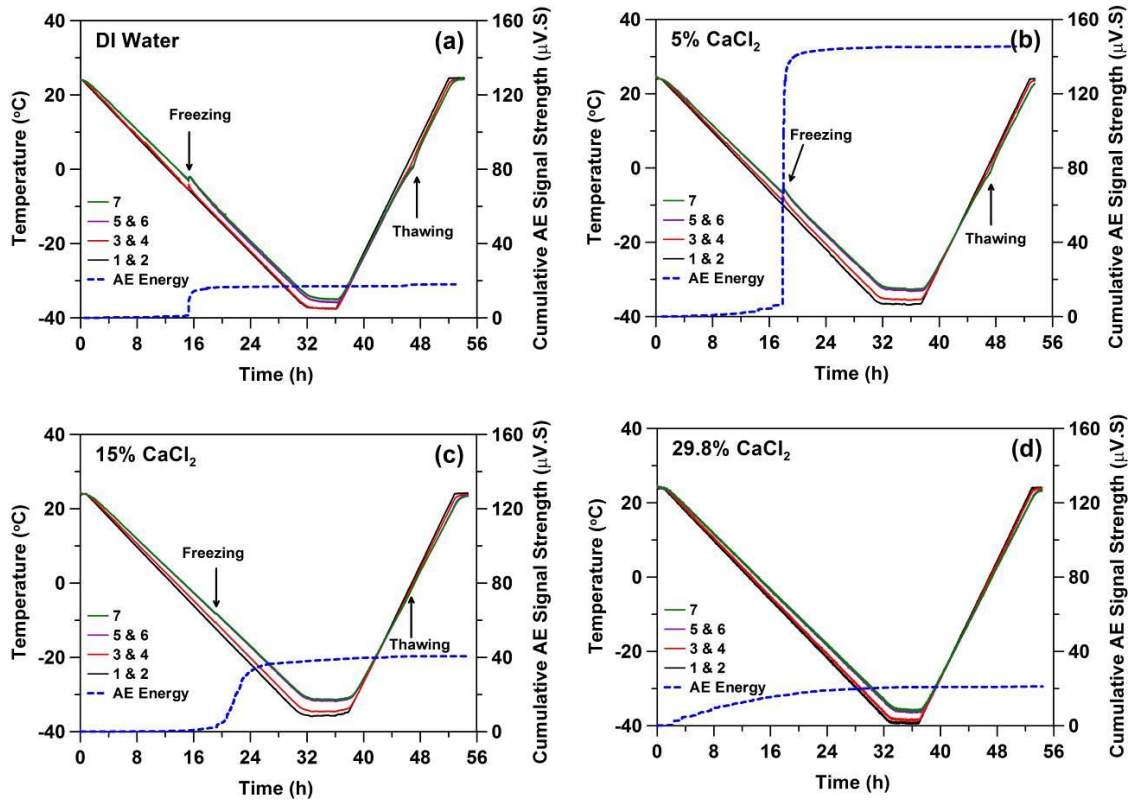
Figure 2 - Temperature at different locations (1 & 2: temperature between cold plate and bottom meter bar; 3 & 4: temperature between bottom meter bar and specimen; 5 & 6: temperature between specimen and top meter bar; and 7: temperature at the top surface of top meter bar), and total cumulative AE signal strength versus time during freeze-thaw cycle for specimens saturated with (a) DI water, (b) 5 % $CaCl_2$ solutions, c) 15 % $CaCl_2$ solutions, and d) 29.8 % $CaCl_2$ solutions.

No freezing and melting peaks were detected by measured heat flow for specimens saturated by solutions with concentrations greater than 20 % $CaCl_2$. Additionally, for a specimen saturated with 20 % $CaCl_2$, only an observed exothermic peak (associated with freezing) is reported. This can be due to the small amount of heat absorbed during gradual melting that was not detected.
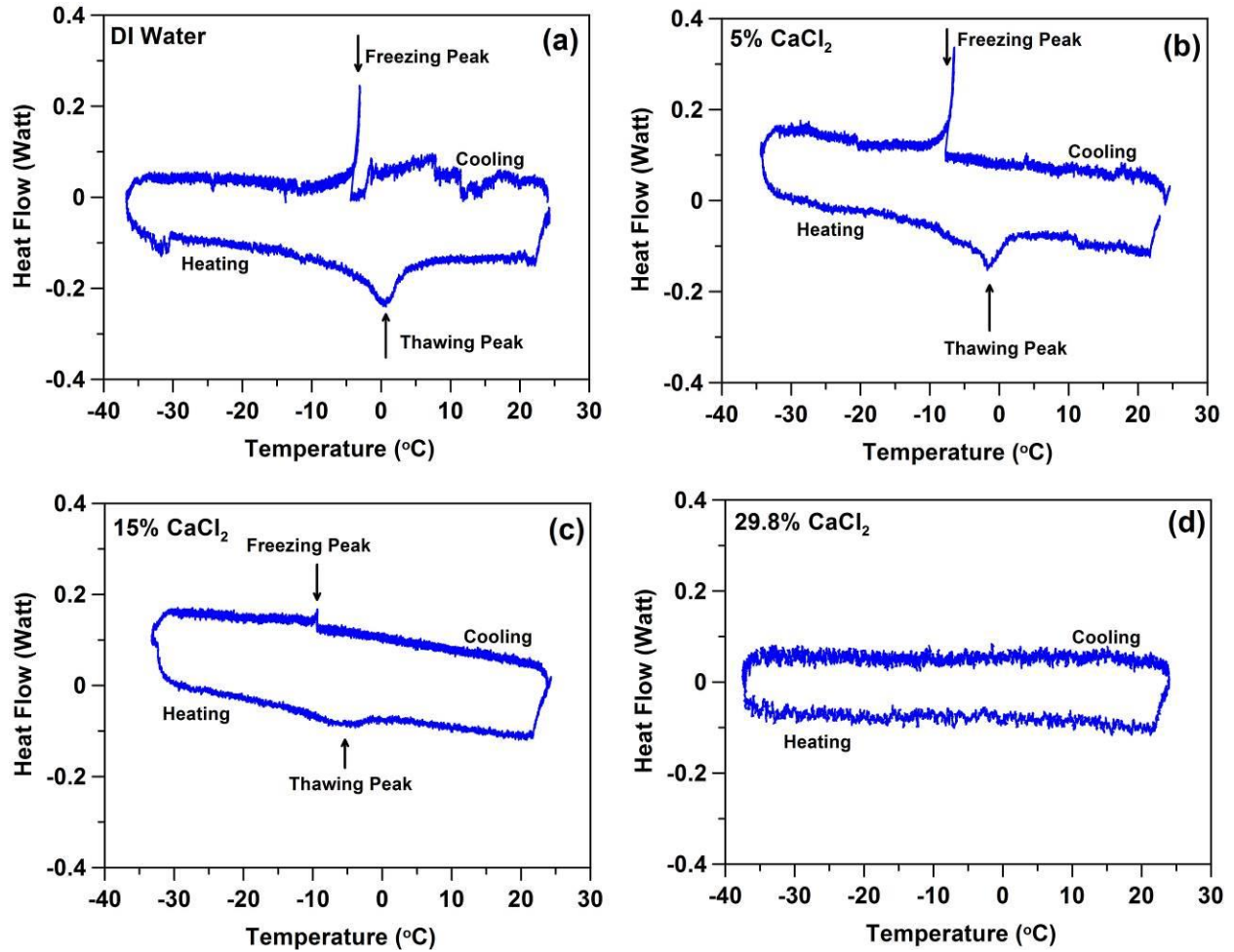
Figure 3 - Heat flow inward/outward of mortar specimen versus temperature during freeze-thaw cycle for mortar specimens saturated with (a) DI water; (b) 5% CaCl$_2$ solution; (c) 15 % CaCl$_2$ solution; and, (d) 29.8 % CaCl$_2$ solution.
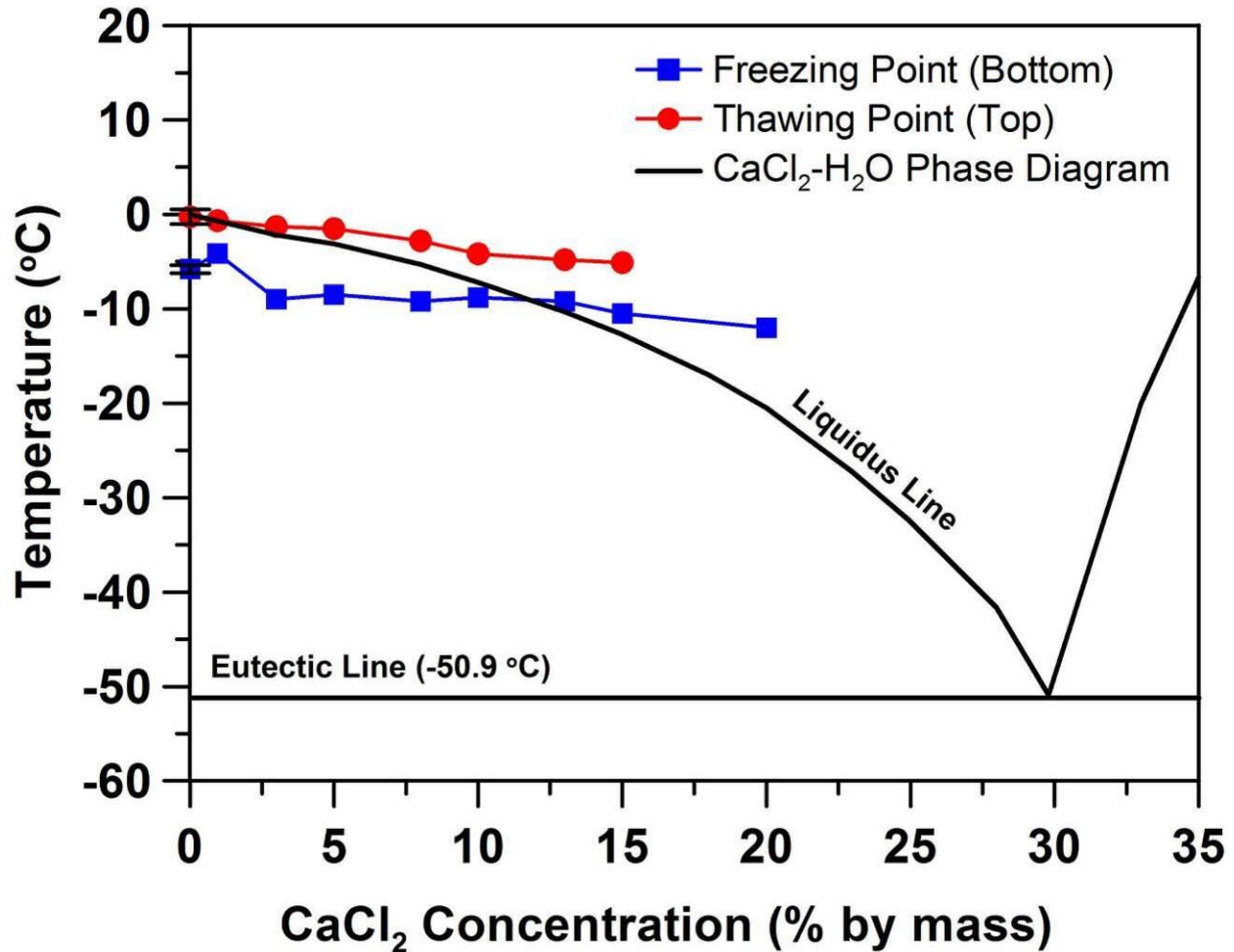
Figure 4 - Freezing and melting points of mortar specimens saturated with different $CaCl_2$ solutions obtained by AE-LGCC compared to the phase diagram of $CaCl_2$ solution.

After vacuum saturation, the volume fraction of absorbed solution for every specimen (i.e., the volume of absorbed solution after vacuum saturation divided by the volume of the specimen) was calculated and normalized by the volume fraction of absorbed solution for the specimen saturated by DI water to determine a normalized degree of saturation (DOS). The normalized DOS is shown in Table 2. It also shows the temperatures at which freezing and melting were detected (Figure 4). The normalized DOS achieved after vacuum saturation shows a very sharp reduction in specimens saturated by the higher concentrations of $CaCl_2$ solutions (20 %, 25 %, and 29.8 %). The reduction in the normalized DOS shows that the amount of liquid phase (solution) in the specimen decreases as the concentration of $CaCl_2$ solution increases. The smaller amount of liquid phase present in the specimens saturated with 20 %, 25 %, and 29.8 % $CaCl_2$ solutions will generate/absorb a smaller amount of heat during any freezing/melting. This supports the detection of no freezing and melting peaks for specimens (only partially) saturated by solutions with concentrations greater than 20 % $CaCl_2$.

The very sharp reduction in the volume fraction of absorbed solution for higher concentrations (despite the fact that a vacuum saturation technique was used for saturating specimens) may indicate the formation of a phase/phases that can block the specimen pores;

11

thereby preventing further penetration of solution into the specimen pores [24]. To determine the depth of penetration, specimens saturated by higher concentrations of $CaCl_2$ solutions were broken at their mid-length and images from mid cross sections were taken immediately after their freeze-thaw experiment. In addition, images were taken after spraying a 0.1 mol/L silver nitrate solution on their surface (Figure 5). The depth of penetration is indicated by the areas with a white color.

While the specimens saturated with concentrations up to 15 % $CaCl_2$ solution showed the fluid ingress throughout the entire cross section of the mortar sample, specimens saturated by higher concentrations showed partial fluid ingress in the sample, meaning the solution did not penetrate to the center of the sample because of blocked pores (Figure 5). The cores of specimens saturated by 25 % and 29.8 % appeared to be dry, providing further evidence that pores near the specimen surfaces may be blocked by an expansive chemical reaction (such as calcium oxychloride formation), thereby preventing further fluid ingress into these specimens. The images after exposure to the silver nitrate solution indicate a similar trend; chloride ions are found near the specimen surface due to the formation of chloroaluminate phases or calcium oxychloride. It should be noted that the viscosity and the surface tension for $CaCl_2$ solution change as the $CaCl_2$ concentration increases [45]; and this may also reduce the fluid ingress. However, it is reported that changes in viscosity and the surface tension are not the main causes and the formation of the chemical phases (chloroaluminate phases and calcium oxychloride) is the dominant reason for reduction in $CaCl_2$ fluid ingress into mortar specimens [24].

Table 2- Normalized degree of saturation (DOS) for mortar specimens after vacuum saturation; and temperatures at which freezing and melting were detected.

Solution Concentration (%)	Solution Properties		Specimen Mass (g)[++]		Absorbed Solution (% by Volume)[*]	Normalized DOS	Temperature of Specimen (°C)[++]		Amount of supercooling w.r.t. $CaCl_2$-H_2O liquidus line
	Freezing Point (°C)	Density at 25 °C (kg/m³)	Dry	Wet			Freezing Point	Melting Point	
0	0	997	70.97	77.78	20.9	1.01	-6.1	0.3	-6.1
			72.96	79.86	20.2	0.99	-5.5	-0.8	-5.5
0.96	-0.5	1005	70.64	77.46	20.6	1.00	-4.2	-0.7	-3.6
3	-2.2	1021	69.80	76.73	20.6	1.00	-9.0	-1.3	-6.8
5	-4	1042	71.56	78.45	19.5	0.95	-8.5	-1.5	-4.5
8	-5	1065	71.82	78.93	19.9	0.97	-9.2	-2.8	-4.2
10	-7	1087	71.21	78.19	19.3	0.94	-8.8	-4.2	-1.8
13	-10	1110	68.67	75.92	20.4	0.99	-9.2	-4.8	+1.0
15	-12	1139	70.83	78.28	19.7	0.95	-10.5	-5.1	+1.5
20	-20	1189	70.35	76.85	16.5	0.80	-12.0	-[**]	+8.0
25	-32	1240	71.70	76.03	10.4	0.50	-[+]	-[+]	-
29.8	-49	1291	70.09	73.06	6.9	0.33	-[+]	-[+]	-

[*] The volume of absorbed solution after vacuum saturation divided by the volume of the specimen.
[**] For this specimen, only an exothermic peak (freezing) was observed while no endothermic peak (melting) was observed.
[+] No freezing and melting peaks were detected for these specimens.
[++] Mass measurements were made to the nearest 0.01 g and temperatures were measured to the nearest 0.2 °C
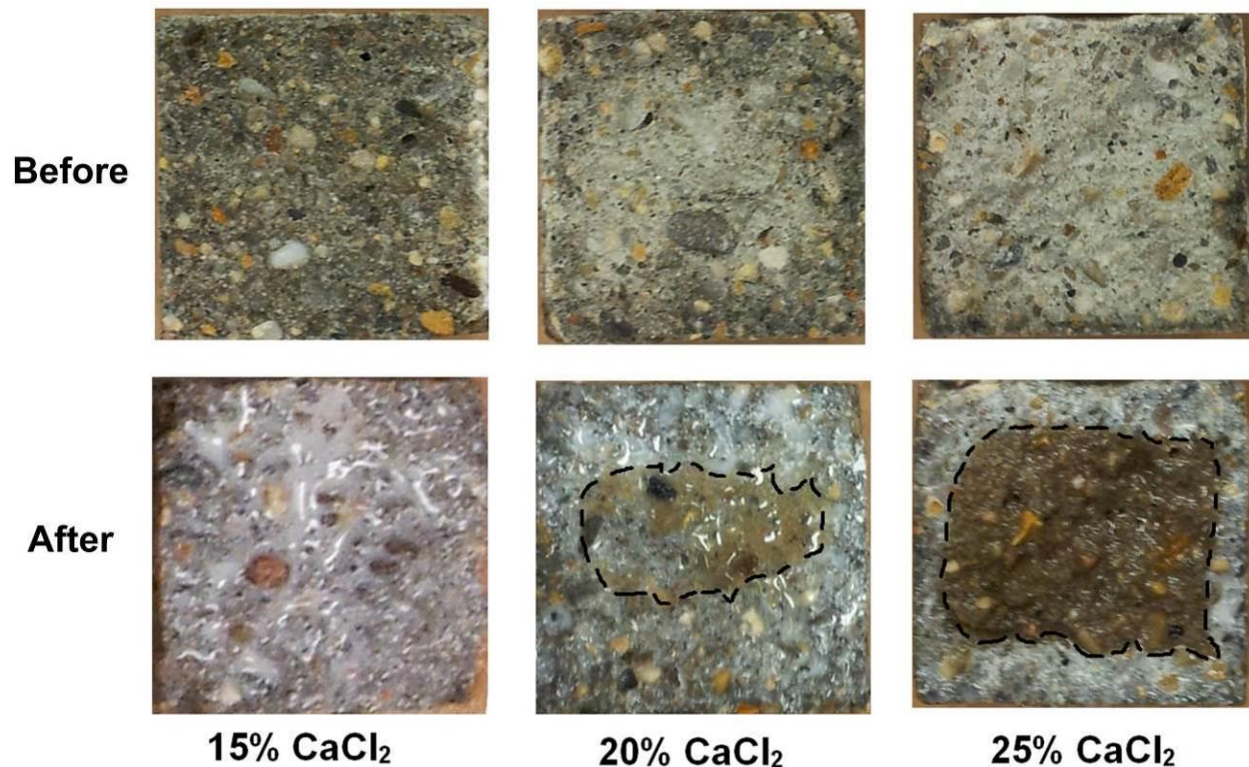
Figure 5 - Mid-length cross section images of specimens saturated by 15 %, 20 %, and 25 % $CaCl_2$ solution immediately after freeze-thaw test: before spraying 0.1 M silver nitrate solution (top), and after spraying 0.1 M silver nitrate solution (the dashed line was added to better indicate the boundary between two regions).

3.2   Concrete Degradation and Freeze-Thaw Damage (AE-LGCC Experiment)

Acoustic activity was monitored during the AE-LGCC experiment to determine damage due to cracking in the mortar specimens caused by phase changes (i.e., due to the expansion caused by either ice formation or calcium oxychloride precipitation). The cumulative AE signal strength was calculated and used as an indication of the magnitude and the time of cracking. Cumulative AE signal strength as a function of time is indicated in Figure 2for samples saturated with 0 %, 5 %, 15 %, and 29.8 % $CaCl_2$ solutions. When the freezing begins to occur, AE cumulative signal strength rises, indicating that cracking is taking place due to the expansion caused by the ice formation inside specimen pores (Figure 2a, Figure 2b, and Figure 2c). However, AE signal strength begins to increase for specimens saturated by 20 %, 25 % and 29.8 % $CaCl_2$ solution from the onset of the AE-LGCC test (29.8 % solution data in Figure 2d), while the temperature of the specimen was maintained at 24 °C for equilibration. This is due to the fact that the chemical reactions (mainly calcium oxychloride formation) begin to occur as soon as the specimen is exposed to 20 %, 25 % and 29.8 % $CaCl_2$ solutions, causing cracking and damage at room temperature.

Figure 6 indicates AE activities (amplitude of events) as a function of temperature for specimens saturated by DI water, 5 %, 15 %, and 29.8 % $CaCl_2$ solutions. For lower concentrations, clusters of AE events occur at the freezing/melting temperatures. The AE activity becomes more scattered as the solution concentration increases.

For higher concentrations (i.e., 20 %, 25 % and 29.8 %), AE events were detected from the onset of the AE-LGCC test (Figure 6d). AE events have higher amplitude at earlier times, during

the time when the specimen was removed from the solution and placed in the AE-LGCC. The amplitude of AE events decreases over time; this may be attributed to the consumption of $CaCl_2$ solution due to the formation of chemical phases over time. In fact, calcium oxychloride may be a main cause of cracking (or AE activity) due to the volume increase that accompanies its formation.

The relative dynamic modulus, E_t/E_o (the ratio of the dynamic modulus at time t, E_t, to the initial or reference dynamic modulus, E_o), is often used to calculate the damage index ($1-E_t/E_o$) in mortar specimens when cracking takes place. It has been shown that dynamic modulus is related to the square of the pulse velocity transmitted through the concrete/mortar specimens [42].

Mortar specimens saturated by 20 %, 25 %, and 29.8 % $CaCl_2$ solutions indicated a reduction in their pulse velocity even before the freeze-thaw experiment. Therefore, a damage index was calculated for these mortar specimens after saturation and immersing in $CaCl_2$ solutions (i.e., before the AE-LGCC experiment). In this case, the dynamic elastic modulus for a specimen saturated by DI water was considered as a reference dynamic modulus (E_o). The calculated damage index is shown in **Figure** Figure 7a.
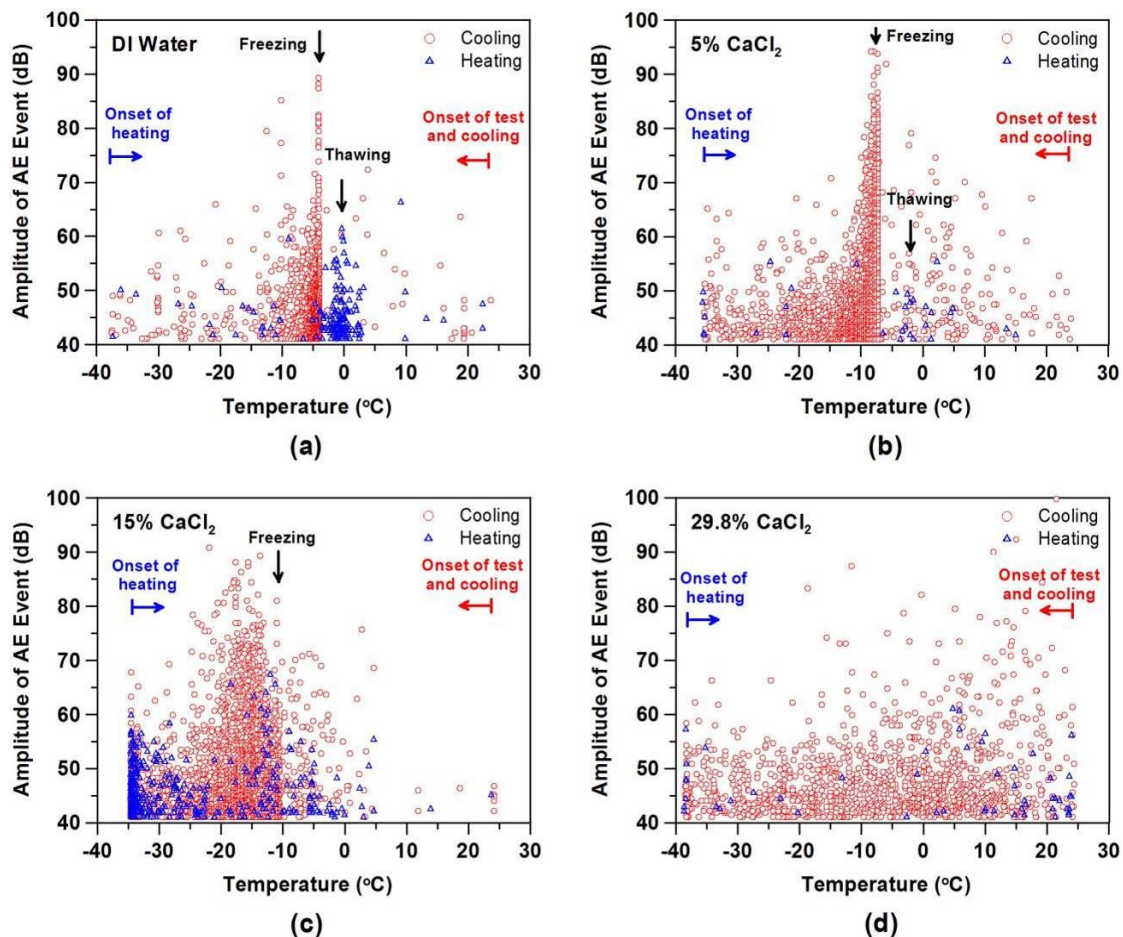

Figure 6 - Passive AE events versus temperature during cooling and heating for mortar specimens saturated with (a) DI water; (b) 5 % $CaCl_2$ solution; (c) 15 % $CaCl_2$ solution; and (d) 29.8 % $CaCl_2$ solution (scattered AE activity can be seen for the 29.8 % concentration).

For specimens saturated by solutions with concentrations less than 20 % CaCl$_2$, almost no damage was observed prior to freezing. However, mortar specimens saturated by 20 %, 25 %, and 29.8 % CaCl$_2$ solutions showed a reduction of more than 20 % in their dynamic elastic modulus, even as the temperature remained constant at 23 °C. When the specimens were immersed in the solution with 20 %, 25 %, and 29.8 % CaCl$_2$ concentrations, some degradation was also seen at the edges of mortar specimens prior to the AE-LGCC experiment (Figure 8). It was observed that the degradation at the specimen edges increases as the immersion time increases. All specimens were kept in the solution for 3 d to be consistent throughout the AE-LGCC experiment. The damage caused by immersing specimens in high concentration solution is most likely attributed to the formation of expansive calcium oxychloride. The reduction in pulse velocity is most likely attributed to the fact that the cores of these specimens were almost dry, because a pulse has a higher velocity in a fully saturated uncracked specimen than in a partially saturated and cracked specimen.
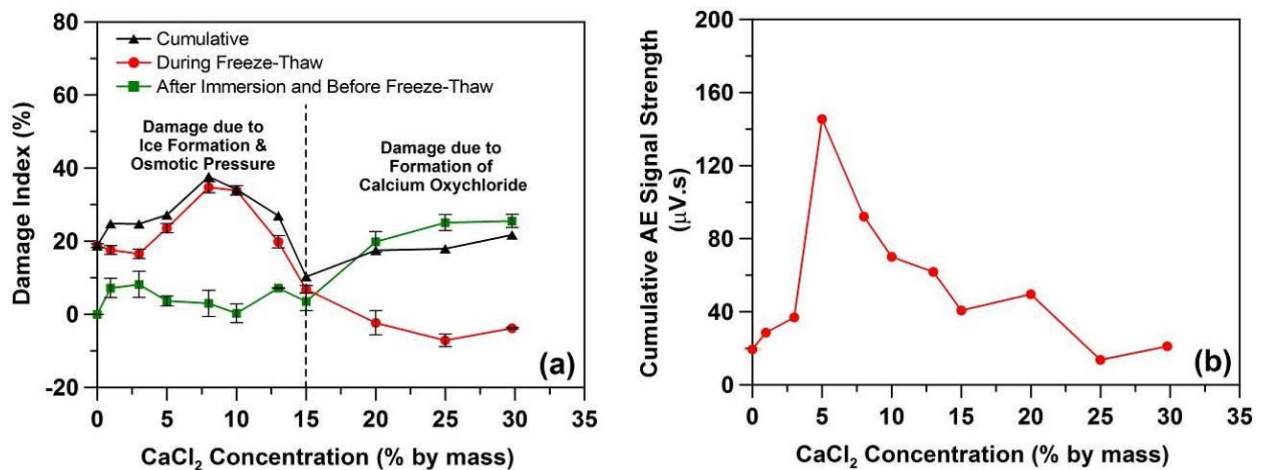

Figure 7 - a) Change in the dynamic elastic modulus and damage index due to immersion in CaCl$_2$ solution and one freeze-thaw cycle; and b) cumulative AE signal strength due to one freeze-thaw cycle for specimens saturated with different dosages of CaCl$_2$ solution (the error bars indicate ± one standard deviation for two replicates of pulse velocity testing).

Dynamic elastic modulus determined for specimens before (E_o) and after (E_t) the freeze-thaw test and the associated damage index is indicated in Figure 7a. The cumulative damage index was also calculated as the sum of these two damage indices and is shown in this figure. While specimens saturated by solutions with higher concentrations (20 %, 25 %, and 29.8 %) showed more damage during immersion time, they showed relatively no increase in damage after the freeze-thaw test. This may be attributed to the relatively low DOS in these samples (i.e., the specimens may have a DOS less than the critical degree of saturation). In addition, it seems that only a small amount of calcium oxychloride was subsequently formed during the AE-LGCC experiment, inducing relatively less deterioration. In fact, the continuous presence (replenishing) of high concentration solution is essential for continuous calcium oxychloride formation. As the specimens were removed from solution to perform the AE-LGCC experiment, the formation of calcium oxychloride decreased during time (Figure 6d).

Figure 7b shows the total cumulative AE signal strength as a function of solution concentration. Samples saturated by solutions with concentration between 5 % and 10 % showed a higher level of freeze-thaw damage and cumulative AE signal strength. This can be

attributed to the critical damage caused by a combination of hydraulic pressure (ice formation) and osmotic pressure during freeze-thaw cycles [6,46].

Figure 8 - Damage at the edges of mortar specimens immersed in a 29.8 % CaCl$_2$ solution prior to the AE-LGCC experiment (arrows highlight the damage and degradation).

3.3   Chloride Profile and Fluid Ingress within the Depth of Mortar Specimens (XRF Experiment)

The XRF experiment was conducted to estimate the chloride profile within the depth of mortar specimens. Color-coded XRF image maps for elemental chlorine are shown in Figure 9, with all images normalized to a single color scale. Areas of highest chlorine concentration are colored in white and yellow, while areas of lower chlorine concentration are colored in red. In addition, areas with no chlorine concentration are colored in black. As expected, a similar pattern of chlorine was observed in XRF images and in the images where the samples were sprayed with the 0.1 mol/L silver nitrate solution.

The XRF elemental chlorine images show the chlorine distribution within the mortar specimens. The color changes from black to yellow/white as the concentration of solution used for saturation increases. While specimens saturated by solutions with CaCl$_2$ concentrations less than 25 % showed the presence of chlorine in their entire cross-section, specimens with 25 % and 29.8 % had no chlorine in their center (i.e., core of specimen).

For concentrations less than 15 %, a constant color gradient is observed throughout the whole section, indicating that the solution was able to penetrate inward through the specimen pores. For concentrations greater than 15%, a gradient of chlorine concentration can be observed through the specimen depth. This may indicate that at room temperature (23 °C), chemical phases (i.e., chloroaluminate phases and calcium oxychloride) begin to form when the concentration of CaCl$_2$ solution is more than 15 % (assuming 100 % of relative humidity as the specimens were vacuum immersed in the solution). For concentrations equal to 25 % and 29.8 %, it seems that the rapid formation of chemical phases at the surface of the specimens during vacuum saturation prevents the further ingress of chlorine into the specimen as both of

16

these exhibit significantly lower chloride concentrations (in the specimen center) than the 20 % specimen.
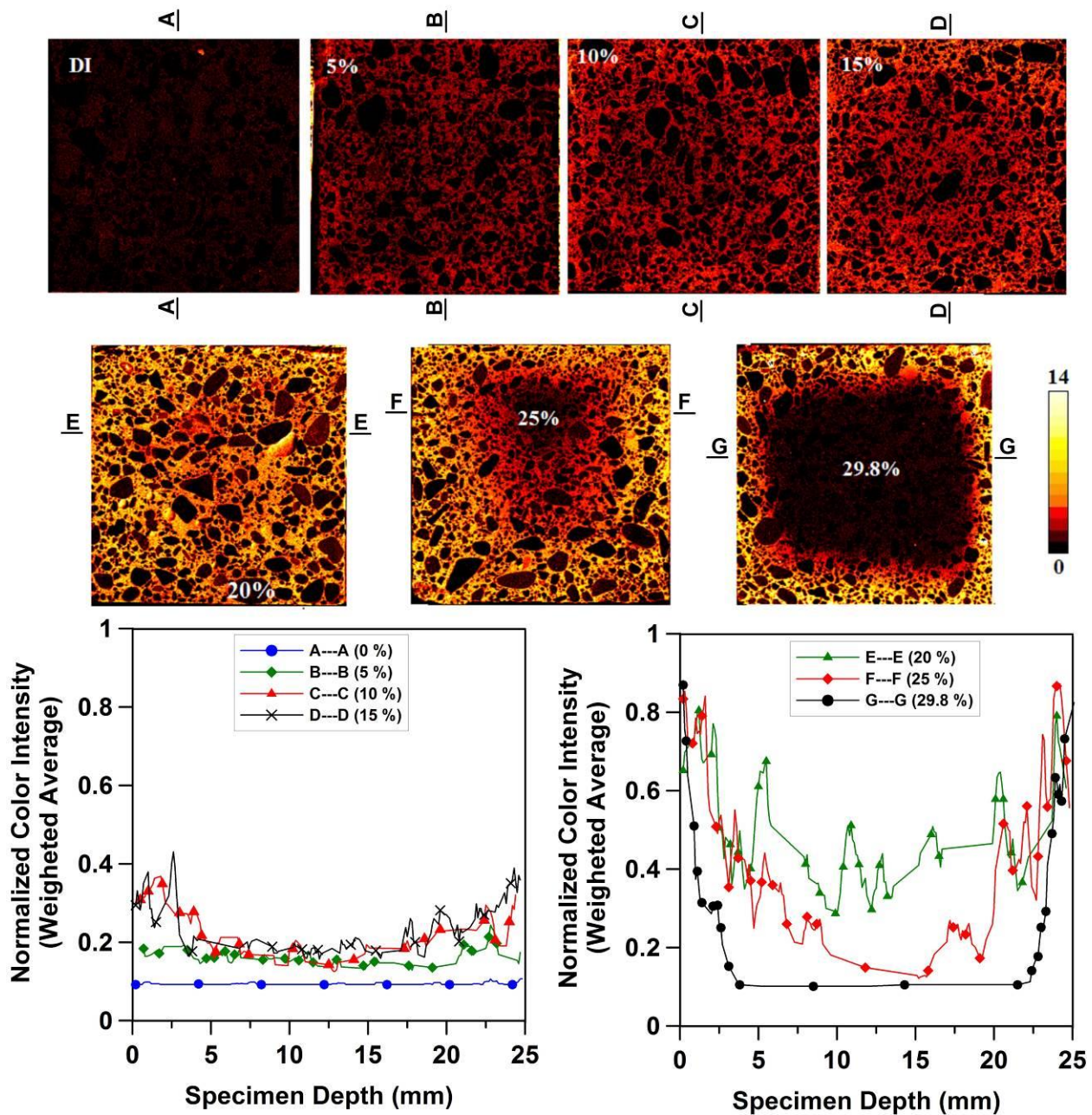

Figure 9 - X-ray fluorescence images alongside normalized color intensity plots for mortar specimens saturated by solution with different concentration of $CaCl_2$ by mass (scale bar indicates the intensity of chlorine content in which 0 and 14 represent no chlorine content and the highest chlorine content, respectively; and aggregate color intensity was not considered in the normalized plots).

3.4   Phase Change Determination (LT-DSC Experiment)

Different series of experiments were performed using the LT-DSC to determine the temperature at which phase changes occur for Series I: $CaCl_2$ solution, Series II: pore solution, Series III- $Ca(OH)_2$ powder with a $Ca(OH)_2:CaCl_2$ molar ratio greater than 3, Series IV: $Ca(OH)_2$ powder with a $Ca(OH)_2:CaCl_2$ molar ratio equal to or less than 3, and Series V: hydrated cement (powder specimen). Specifically, the results from this section were used to determine the temperature at which calcium oxychloride (which can be very destructive) forms in cementitious materials.

3.4.1   Heat flow response versus temperature

Figure 10 provides an example of data for specimens with 20 % $CaCl_2$ concentration to compare the LT-DSC heat flow behavior during heating as a function of temperature for five series of LT-DSC experiments. For the $CaCl_2$ solution case (Series I), two endothermic peaks were observed corresponding to the moment that the eutectic solid melts (i.e., ~ -50.8 °C which is shown with "a" mark in the figure) and the range of temperatures over which the ice is melting as shown with "b" mark in the figure. For the pore solution case (Series II), in addition to the peaks associated with eutectic solid melting and ice melting, four additional endothermic behaviors were observed (shown with arrows in the figure). For $Ca(OH)_2$ powder with a $Ca(OH)_2:CaCl_2$ molar ratio equal to 1 (Series IV), in addition to the peaks associated with eutectic solid melting and ice melting, an endothermic behavior (shown with "c" mark in the figure) appeared at a temperature above 0 °C that most likely corresponds to the chemical phase transition for the calcium oxychloride [31,35,36]. It should be mentioned that chloroaluminate phases (such as Friedel's salt) are stable until the temperature of the sample reaches near 200 °C [47] and the endothermic behavior observed at a temperature above 0 °C is therefore most likely calcium oxychloride melting. The eutectic solid melting peak seems to become very small for $Ca(OH)_2$ powder with a $Ca(OH)_2:CaCl_2$ molar ratio equal to 3. The eutectic solid melting peak disappeared for $Ca(OH)_2$ powder with a $Ca(OH)_2:CaCl_2$ molar ratio greater than 3 (Series III). Hydrated cement powder (Series V) behaved relatively similar to $Ca(OH)_2$ powder with a $Ca(OH)_2:CaCl_2$ molar ratio equal to 1.

Table 3 summarizes the temperatures associated with the eutectic solid melting, the ice melting, and the calcium oxychloride melting for five series of LT-DSC experiments for specimens with 20 % $CaCl_2$ concentration. The temperature associated with eutectic solid melting remains somewhat unchanged near the melting point for $CaCl_2$-H_2O eutectic solid (i.e., -50.8 °C) for LT-DSC experiments of specimens with a 20 % $CaCl_2$ concentration, since eutectic solid almost always melts at a constant temperature [47]. The temperature at which ice melting terminates (i.e., liquidus temperature), however, depends on the $CaCl_2$ concentration in the solution and as the $CaCl_2$ concentration increases, the liquidus temperature reduces [47]. Table 3 and Figure 10 show a substantial change in the liquidus temperature for LT-DSC experiments of specimens with 20 % $CaCl_2$ concentration; this is mainly due to the fact that $CaCl_2$ from solution is used to form calcium oxychloride and as a result the concentration of $CaCl_2$ in the solution is reduced by the calcium oxychloride formation causing an increase in the liquidus temperature.
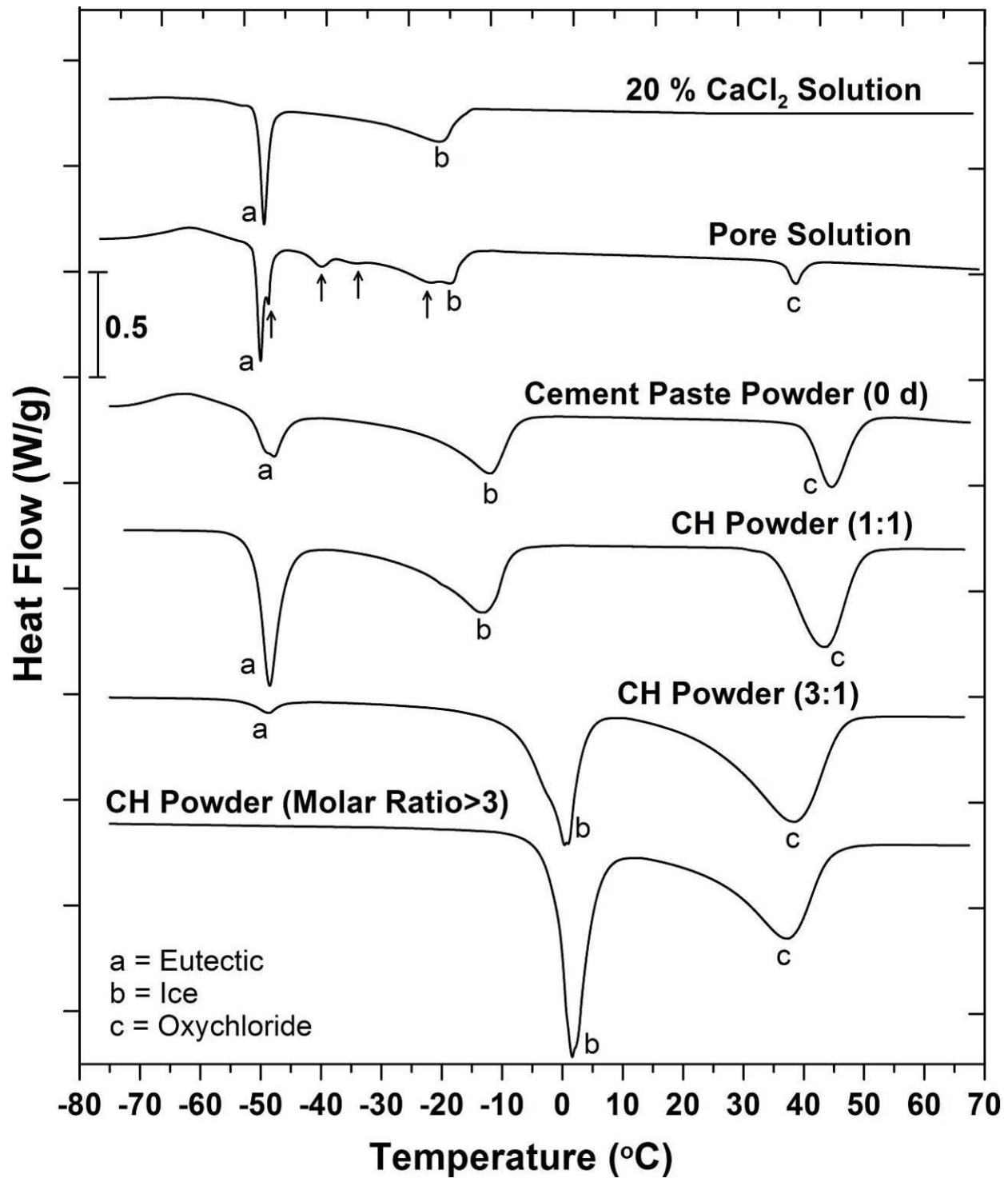
Figure 10 - Heat flow during heating versus temperature for five series of LT-DSC experiments for specimens with 20 % $CaCl_2$ concentration (heat flow is normalized by the total mass of specimen including powder plus solution).

Table 3- The temperatures associated with eutectic solid melting (shown with "a" mark in Figure 10), ice melting (shown with "b" mark in Figure 10), and calcium oxychloride melting (shown with "c" mark in Figure 10) for five series of LT-DSC experiments for specimens with a 20 % $CaCl_2$ concentration (notice that the temperature associated with the maximum of each peak is reported).

LT-DSC Experiment	Eutectic Solid (°C)	Ice (°C)	Calcium Oxychloride (°C)
$CaCl_2$ solution (Series I)	-49.4	-20.4	-*
Pore solution (Series II)	-50.0	-18.8	38.7
$Ca(OH)_2$ powder with $Ca(OH)_2$:$CaCl_2$ molar ratio more than 3 (Series III)	-	1.6	37.1
$Ca(OH)_2$ powder with $Ca(OH)_2$:$CaCl_2$ molar ratio equal to 1 (Series IV)	-48.5	-13.3	43.6
$Ca(OH)_2$ powder with $Ca(OH)_2$:$CaCl_2$ molar ratio equal to 3 (Series IV)	-48.8	0.3	38.4
Hydrated cement paste powder, 0 d (Series V)	-47.8	-12.0	44.7

* Not available

3.4.2 Interaction between $CaCl_2$ and Pore Solution (Series I and II)

NaOH and KOH in concrete pore solution can interact with $CaCl_2$ solution and alter the behavior that one might expect based on the conventional $CaCl_2$-H_2O phase diagram. In fact, NaOH and KOH may add additional phases to the conventional $CaCl_2$-H_2O phase diagram which is shown in Figure 11. The eutectic and liquidus temperatures (i.e., temperatures associated with eutectic solid melting and ice melting, respectively) for $CaCl_2$ solution are shown in Figure 11a as the salt concentration increases. The experimental results reasonably followed the $CaCl_2$-H_2O phase diagram from Figure1a. Figure 11b shows the comparison of temperatures corresponding to different endothermic behaviors that were found for pore solution with the $CaCl_2$-H_2O phase diagram. For pore solution, the liquidus and eutectic temperatures follow the $CaCl_2$ solution phase diagram. The endotherm that was observed at a temperature greater than 0 °C is compatible with the calcium oxychloride liquidus line which will be discussed later in the $Ca(OH)_2$-$CaCl_2$-H_2O phase diagram (Figure 12) (and isoplethal sections). The presence of calcium oxychloride in pore solution shows that alkalis in pore solution (i.e., NaOH and KOH) react with $CaCl_2$ in the presence of water, and produce $Ca(OH)_2$, NaCl, and KCl. $Ca(OH)_2$ produced by this reaction can further react with $CaCl_2$ (as a secondary reaction) and form calcium oxychloride. In fact, consumption of alkalis in pore solution can reduce the pH of concrete pore solution, which was observed elsewhere [16,22]. It should be mentioned that the four additional endotherms that were also observed for pore solution (shown by arrows in Figure 10) may be attributed to the phase changes due to the presence of NaCl and KCl salts, generated via the above-mentioned reactions in pore solutions.
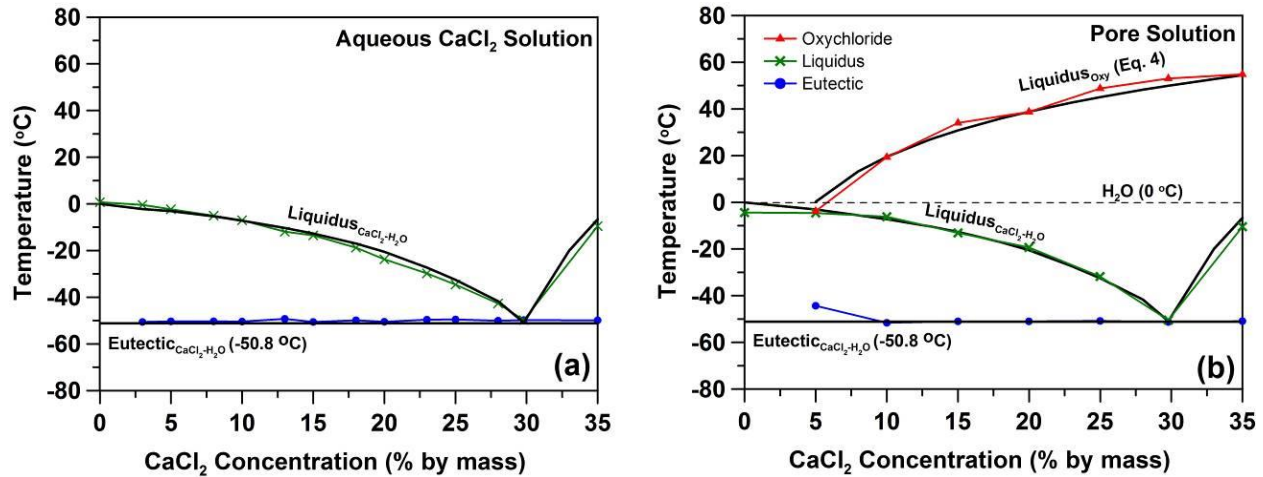
Figure 11 - Comparison of temperatures associated with different endotherms observed in LT-DSC during heating with aqueous $CaCl_2$ phase diagram as a function of $CaCl_2$ concentration for: a) $CaCl_2$ solution, b) pore solution containing $CaCl_2$ salt (notice that the four additional endotherms observed for pores solution, shown by arrows in Figure 10, were not reported in this plot)[1].

3.4.3 Isoplethal Sections for $Ca(OH)_2$-$CaCl_2$-H_2O Ternary Phase Diagram and Formation Temperature for Calcium Oxychloride (Series III and IV)

The LT-DSC results for $Ca(OH)_2$ powder as a function of $CaCl_2$ concentration are shown in Figure 12. The $Ca(OH)_2$-$CaCl_2$-H_2O isoplethal section of the phase diagram varies as the $Ca(OH)_2$:$CaCl_2$ molar ratio changes. When a similar mass amount of $Ca(OH)_2$ powder and solution were blended and tested in LT-DSC (i.e., an isoplethal section of $Ca(OH)_2$-$CaCl_2$-H_2O ternary phase diagram when the $Ca(OH)_2$:$CaCl_2$ molar ratio is greater than 3), only two endothermic behaviors were detected, corresponding to calcium oxychloride liquidus and water/ice phase changes, respectively (Figure 12a). In specimens with a molar ratio more than 3, all of the $CaCl_2$ in the solution is used by the formation and precipitation of calcium oxychloride at temperatures above 0 °C. As a result, no $CaCl_2$ remains in the solution and the remaining pure water transforms to ice at 0 °C.

A logarithmic trend line is fitted to the data points (temperature versus $CaCl_2$ concentration) at which calcium oxychloride forms/melts and is presented in Eq. 4.

$$T = 27.88 \ln \frac{C_o}{C^*} \qquad\qquad R^2 = 0.99 \qquad\qquad \text{Eq. 4}$$

---

[1] It should be mentioned that the diagrams provided in this study do not always represent a pure phase diagram since they may contain additional compounds and phases. Some diagrams are isoplethal diagrams from an actual phase diagram. These figures provide information to describe how different constituents of a cementitious system (i.e., alkalis, $Ca(OH)_2$, and hydrated cement) can influence the conventional $CaCl_2$-H_2O phase diagram which has been incorrectly used in concrete industry to predict concrete freeze-thaw behavior when exposed to $CaCl_2$ solution.
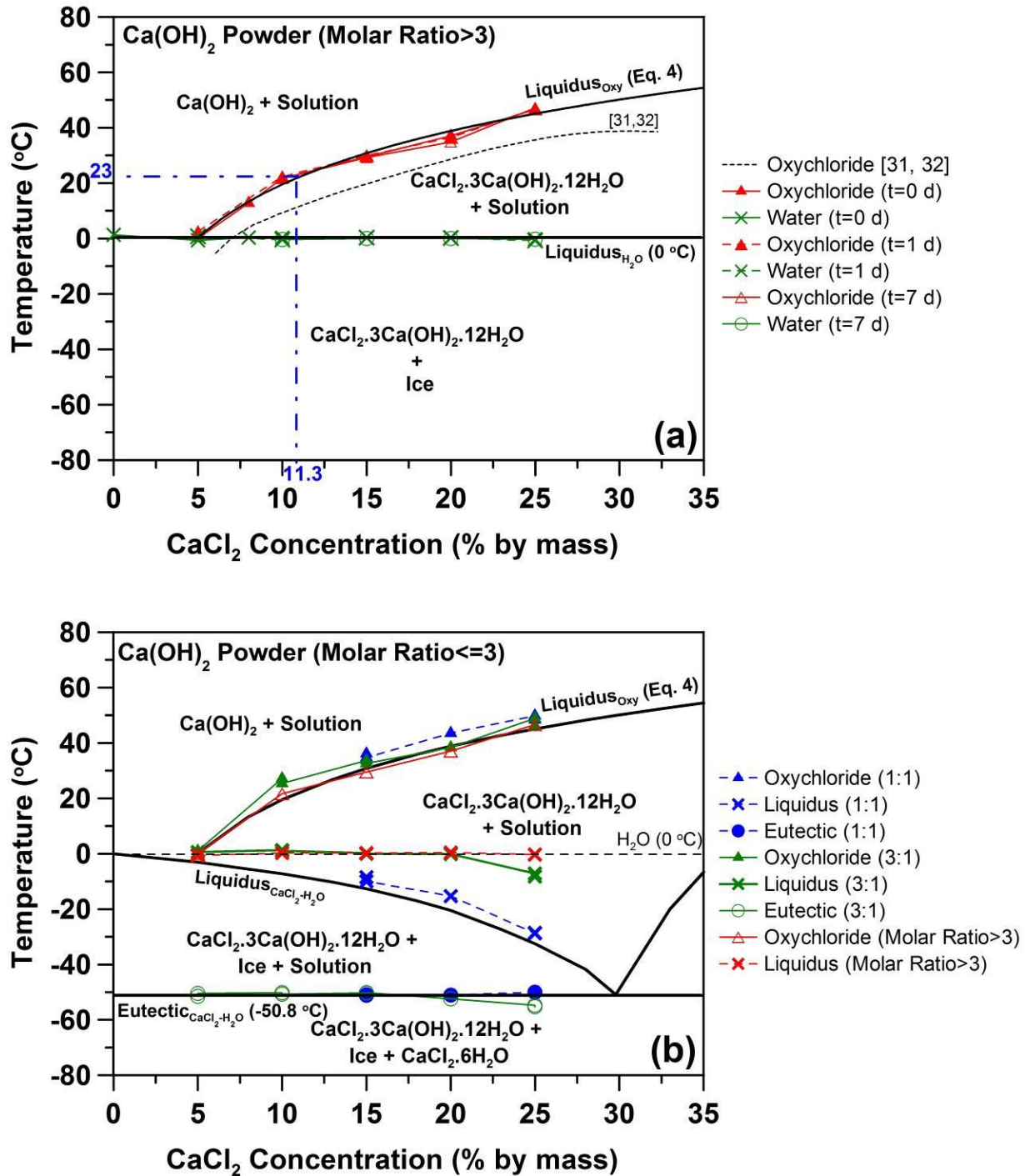
Figure 12 - Isoplethal diagrams of $Ca(OH)_2$-$CaCl_2$-H_2O ternary phase diagram, and the proposed calcium oxychloride formation line due to reaction between calcium hydroxide and $CaCl_2$ solution for a) $Ca(OH)_2$:$CaCl_2$ molar ratio greater than 3, and b) different $Ca(OH)_2$:$CaCl_2$ molar ratios[1].

where T (°C) is the temperature at which calcium oxychloride begins to form/melt, C_o (% by mass) is the initial concentration of $CaCl_2$ solution, and C^* (=4.97 %) is the theoretical minimum concentration of $CaCl_2$ solution for which the calcium oxychloride can be formed.

For $Ca(OH)_2$:$CaCl_2$ molar ratios equal to 3 and 1 (shown in Figure 12b), endothermic behavior associated with the moment that the $CaCl_2$–H_2O eutectic solid melts (~ -50.8 °C) was also detected. This is due to the fact that the total amount of calcium oxychloride that was formed at a higher temperature was not sufficient to consume all of the $CaCl_2$ in the $Ca(OH)_2$-$CaCl_2$-H_2O ternary mixture. As the $Ca(OH)_2$:$CaCl_2$ molar ratio decreases (i.e., 1:1 molar ratio), the endothermic peak associated with the water/ice phase change (liquidus temperatures) moves toward the classical liquidus line for an aqueous $CaCl_2$ solution. In fact, the amount of $Ca(OH)_2$ and the $Ca(OH)_2$:$CaCl_2$ molar ratio changes the liquidus line and eutectic line in the ternary phase diagram (or isoplethal section) containing $Ca(OH)_2$-$CaCl_2$-H_2O.

An interesting observation was that the $Ca(OH)_2$:$CaCl_2$ molar ratio appears to have only a slight effect on the line associated with the calcium oxychloride formation. The line associated with the calcium oxychloride formation reasonably followed Eq. 4 at different $Ca(OH)_2$:$CaCl_2$ molar ratios. It should be noted that for a $Ca(OH)_2$:$CaCl_2$ molar ratio equal to 1, the temperatures at which calcium oxychloride formed were slightly higher than the temperatures obtained for other molar ratios. Using Eq. 4, the critical concentration at which the calcium oxychloride begins to form at room temperature (23 °C) was obtained to be 11.3 %, by mass. For concentrations greater than 11.3 %, the calcium oxychloride forms under laboratory conditions.

3.4.4 Interaction between Hydrated Cement Powder and $CaCl_2$ Solution (Series V)

Figure 13 indicates the temperature associated with different endotherms observed for hydrated cement powder containing $CaCl_2$ solution for different ages after blending. Chloride binding due to the calcium oxychloride formation can be detected since the ice liquidus results moved upward to a higher temperature. As the age of the specimen increases, more binding is taking place and an additional increase in the ice liquidus temperature was observed. This is also evident in the temperatures that eutectic solid melts: at lower concentrations, eutectic solid melting disappears as the age of the specimen increases. This indicates that all of the $CaCl_2$ has been consumed by the formation of calcium oxychloride.

The temperature at which calcium oxychloride formed reasonably follows Eq. 4. However, immediately after blending solution and hydrated cement powder (0 d), the temperature at which calcium oxychloride formed was slightly higher than the trend line proposed in Eq. 4. At ages of 1 d and 7 d, the temperature of calcium oxychloride formation returns to the temperature predicted by Eq. 4. This may be due to the formation of an unstable phase change (such as calcium oxychloride with different molar ratios, i.e., $Ca(OH)_2 \cdot CaCl_2 \cdot xH_2O$) or an interaction between hydrated cement paste, unhydrated cement, and $CaCl_2$ solution at 0 d.
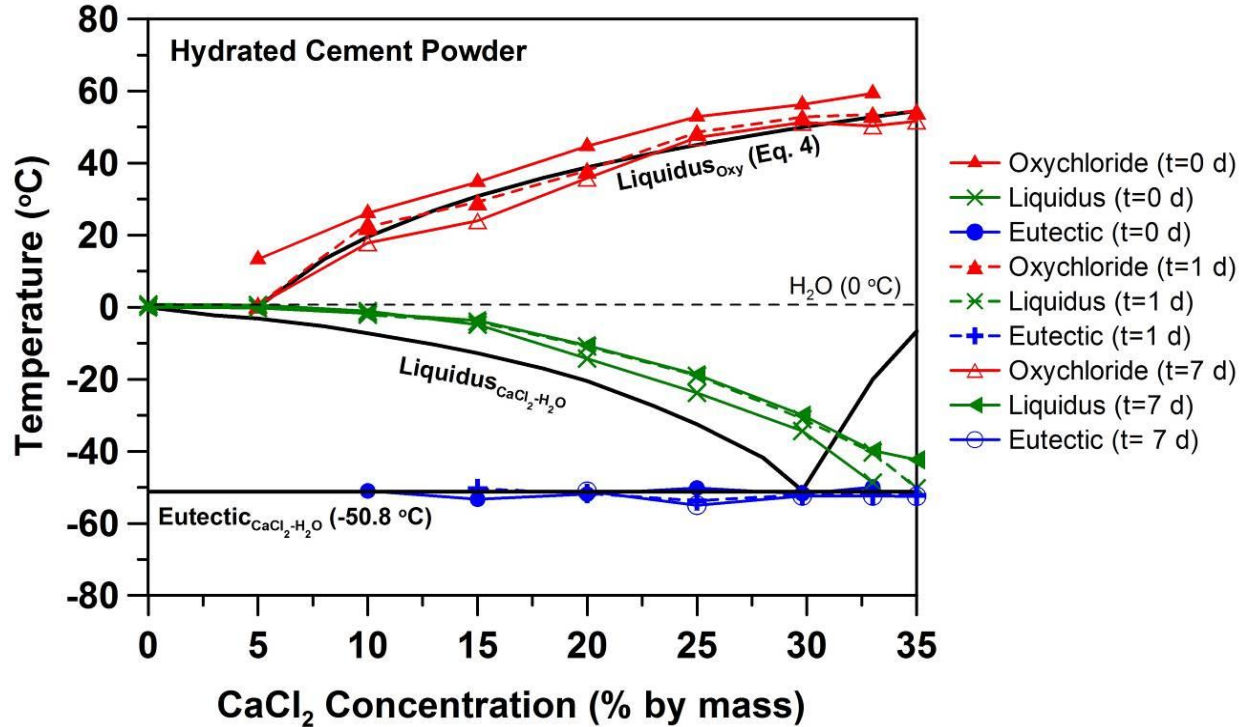
Figure 13 - Comparison of temperatures associated with different endotherms observed in LT-DSC with aqueous $CaCl_2$ phase diagram as a function of $CaCl_2$ concentration for hydrated cement powder blended with $CaCl_2$ solution at different exposure ages[1].

3.5 Rate of Formation for Calcium Oxychloride (IMC Experiment)

Isothermal calorimetry experiments were performed to determine the rate of formation for the calcium oxychloride. Figure 14 shows the heat flow versus time as measured using isothermal micro-calorimetry when a $CaCl_2$ solution was mixed with dry $Ca(OH)_2$ powder or hydrated cement powder. For the hydrated cement powder, the amount of $Ca(OH)_2$ in the paste was determined to be 23.1 % (by mass of dry cement paste) using a thermogravimetric analysis (TGA) method for the cement used in this study at complete hydration [48,49], and the degree of hydration was determined to be 90.4 %.

Blending the $Ca(OH)_2$ powder with a solution that has a concentration less than 15 % showed a very small amount of heat release as illustrated in Figure 14a. This may be attributed mainly to heat release caused by internal mixing. It should be remembered that according to the $Ca(OH)_2$-$CaCl_2$-H_2O isoplethal section (Figure 12), the calcium oxychloride will not form for $CaCl_2$ concentrations less than 11.3 % at the temperature at which the isothermal calorimetry experiment was performed (i.e., 23 °C). Therefore, comparatively no heat of reaction was detected by the experiment for the solutions with concentrations less than 11.3 %. As the concentration of the solution increases (between 15 % and 29.8 % at 23 °C), the heat release increases due to calcium oxychloride formation. The rate of heat release due to calcium oxychloride formation is very rapid and it occurs approximately within first 15 min, illustrating the fast reaction between $Ca(OH)_2$, $CaCl_2$, and H_2O to form calcium oxychloride.
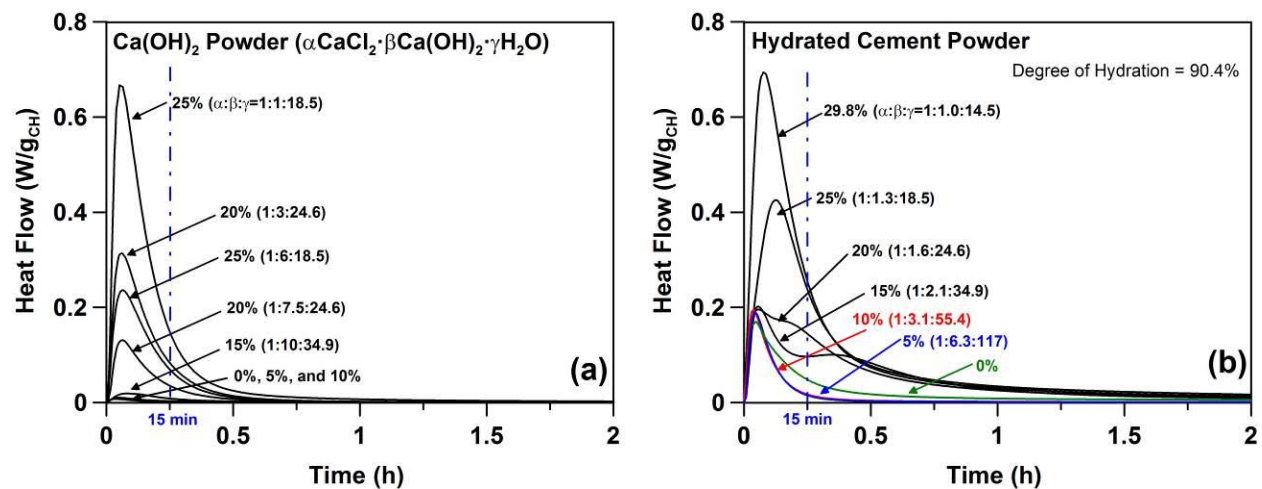
Figure 14 - Isothermal calorimetry heat flow curves (normalized by the amount of Ca(OH)$_2$) versus time for a) Ca(OH)$_2$ powder and CaCl$_2$ solution (for concentrations less than 15 %, very small amount of heat was detected), and b) hydrated cement powder and CaCl$_2$ solution (to calculate the molar ratios, 25.2 % of hydration products was considered to be Ca(OH)$_2$).

For hydrated cement powder (Figure 14b), a relatively similar trend was observed. For 0%, the heat released during the experiment is associated with the heat of hydration of the unreacted cement (or unreacted C$_3$A). For 5 % and 10 %, the heat release is somewhat similar to 0 %, however, the peak becomes slightly narrower since CaCl$_2$ is known as an accelerating agent for cement hydration. For 15% and 20 %, two exothermic behaviors (i.e., a peak with a shoulder) were observed. While the first exothermic behavior was due to unreacted cement hydration, the second exothermic peak is most likely associated with calcium oxychloride formation. As shown in Figure 14b for 15 % and 20 %, the second exothermic peak moved toward the first exothermic peak as the CaCl$_2$ concentration increased. This shows that the rate of reaction between Ca(OH)$_2$, CaCl$_2$, and H$_2$O to form calcium oxychloride increases as the salt concentration increases. For 25 % and 29.8 % the only observed exothermic behavior was the heat released by the combination of unreacted cement hydration and calcium oxychloride formation, observed as a single combined peak.

3.6 The Effect of Ca(OH)$_2$:CaCl$_2$ Molar Ratio on Calcium Oxychloride Formation in Mortar Specimens

It was previously (Section 3.4.3) shown that the Ca(OH)$_2$:CaCl$_2$ molar ratio may change the behavior shown in the isoplethal sections of the Ca(OH)$_2$-CaCl$_2$-H$_2$O system (Figure 12) and the rate of oxychloride formation (Figure 14). The Ca(OH)$_2$:CaCl$_2$ molar ratio can change the liquidus and eutectic lines, while the calcium oxychloride formation line remains relatively unchanged. Thus, in mortar/concrete, it is necessary to calculate the expected Ca(OH)$_2$:CaCl$_2$ molar ratio to predict the freezing point of the CaCl$_2$ solution in the pore structure. It should be noted that in mortar/concrete, there is a limited space for a brine to be absorbed, which is equal to the mortar/concrete porosity. Therefore, the Ca(OH)$_2$:CaCl$_2$ molar ratio is always dictated by both the porosity and paste properties of the mortar/concrete.

The maximum amount of solution that is absorbed by a mortar specimen can be calculated using Eq. 5.

25

$M_{Soln}=\rho_{Soln}\boldsymbol{\times}\Phi$ Eq. 5

where M_{Soln} (kg/m^3) is the maximum mass of absorbed water in a unit volume of mortar specimen, ρ_{Soln} (kg/m^3) is the density of solution at a desired concentration (see Table 2), and Φ is the porosity of the mortar specimen by volume, which was determined to be 20.6 % in this study (see Section 2.2.1).

Additionally, the amount of Ca(OH)$_2$ in mortar specimens can be calculated using Eq. 6.

$M_{CH}=\rho_{paste\ (OD)}\boldsymbol{\times}(V_{paste}/V_{mortar})\boldsymbol{\times}\alpha\boldsymbol{\times}M_{CH/paste}$ Eq. 6

where M_{CH} (kg/m^3) is the mass of Ca(OH)$_2$ in a unit volume of mortar specimen, $\rho_{paste(OD)}$ (kg/m^3) is the density of cement paste in oven dry condition which is determined to be 1574 kg/m^3, (V_{paste}/V$_{mortar}$) is the volume fraction of cement paste in the mortar sample that was obtained as 43.0 % (considering 55 % sand and 4.5 % entrapped air in the mortar sample, by volume) , α is the degree of hydration that was obtained as 77.9 % for the cement paste used in this study to prepare mortar samples (see Section 2.2.1), and $M_{CH/g.s.}$ is the amount of Ca(OH)$_2$ in the dry cement paste by mass at complete hydration that was obtained to be 23.1 % for the cement used in this study (see Section 3.5).

The maximum amount of solution that can be absorbed in mortar specimens, and the amount of Ca(OH)$_2$ that is present in the mortar specimens are shown in Table 4 for various salt concentrations. In addition, the Ca(OH)$_2$:CaCl$_2$ molar ratio and the H$_2$O:CaCl$_2$ molar ratio are calculated and shown in this table. Instead of 25% and 29.8 % CaCl$_2$ concentration, the Ca(OH)$_2$:CaCl$_2$ molar ratio is greater than 3 for all concentrations; this means that the entire amount of CaCl$_2$ can be consumed by the formation of calcium oxychloride in these mortar specimens. For concentrations less than 25 %, the amount of portlandite in mortar is much higher than the amount of Ca(OH)$_2$ that is needed to consume all of the CaCl$_2$ in the absorbed solution and to form calcium oxychloride. Therefore, only pure pore solution remains (as a liquid phase) in mortar pore structures after the formation of calcium oxychloride. This is compatible with what was observed in the freeze-thaw experiments of mortar specimens; in which 1) no depression in freezing/melting temperature was observed, and 2) the temperatures at which freezing/melting occurred were approximately close to the freezing/melting points for water/ice.

For the 20 %, 25 % and 29.8 % CaCl$_2$ concentrations, the calculated Ca(OH)$_2$:CaCl$_2$ molar ratio is relatively close to or less than the molar ratios in the calcium oxychloride formulation (CaCl$_2$•3Ca(OH)$_2$•12H$_2$O). As a result, approximately all the portlandite in cement paste (considering free access to CaCl$_2$ solution during saturation time) can react at a desired temperature to form solid calcium oxychloride. Consumption of the entire amount of Ca(OH)$_2$ and a large portion of CaCl$_2$ solution justifies the observation in freeze-thaw experiments that no exothermic/endothermic peaks were observed due to liquid/solid phase changes during cooling/heating of the mortar specimens saturated with 25 % and 29.8 % CaCl$_2$ concentrations. It should be mentioned that at these concentrations, the calcium oxychloride can be formed at room temperature (Figure 12). The solid calcium oxychloride then precipitates within the mortar pores and the spaces occupied initially by portlandite (solid crystals). This can result in a) internal pressure due to the formation of expansive calcium oxychloride, and b) blocking and filling the mortar pores by this formation, thus reducing the fluid ingress into specimens. Both were seen during the immersion of mortar specimens inside high concentration solutions as a)

degradation was observed on the edges of specimen after 3 d immersion that can be due to internal pressure, and b) it was observed that the exposure solution was unable to penetrate into the specimen despite using a vacuum technique in an attempt to obtain full saturation.

In concrete exposed to $CaCl_2$ solutions, osmotic pressure may also be another cause of damage and scaling issues. In fact, the difference in concentration of solution inside pores that are $CaCl_2$ free solution (i.e., water) and the initial concentration of the solution surrounding the cementitious material can generate a relatively high amount of osmotic pressure. This can further degrade the surface of the cementitious material and cause scaling and damage to the concrete.

Table 4 - $Ca(OH)_2$:$CaCl_2$ and H_2O:$CaCl_2$ molar ratios in mortar specimens for different concentrations of $CaCl_2$ in the solution.

Solution Concentration (%)	Mass (kg/m³)				$Ca(OH)_2$:$CaCl_2$ (Mol/Mol)	H_2O:$CaCl_2$ (Mol/Mol)
	Solution	$CaCl_2$	Water	$Ca(OH)_2$		
0	205.382	0.00	205.38	121.72	-	
0.96	207.03	1.99	205.04	121.72	91.7	635.4
3	210.326	6.31	204.02	121.72	28.9	199.1
5	214.446	10.72	203.72	121.72	17.0	117.0
8	219.39	17.55	201.84	121.72	10.4	70.8
10	223.922	22.39	201.53	121.72	8.1	55.4
13	228.66	29.73	198.93	121.72	6.1	41.2
15	234.634	35.20	199.44	121.72	5.2	34.9
20	244.934	48.99	195.95	121.72	3.7	24.6
25	255.44	63.86	191.58	121.72	2.9	18.5
29.8	265.946	79.25	186.69	121.72	2.3	14.5

4.0 Conclusions

This paper examined how $CaCl_2$ solution influences the behavior of a cementitious matrix under temperature cycling. Isoplethal sections of a ternary phase diagram for a $Ca(OH)_2$-$CaCl_2$-H_2O system were proposed to approximately describe the behavior of a cementitious mortar exposed to $CaCl_2$ deicing salt. These diagrams were used to indicate the temperature at which calcium oxychloride forms. According to the results obtained in this study, the following conclusions can be drawn:

- Isoplethal sections of the $Ca(OH)_2$-$CaCl_2$-H_2O phase diagram were determined from experimental measurements showed that changing the $Ca(OH)_2$:$CaCl$ molar ratio does not appear to significantly influence the temperature at which calcium oxychloride forms. The calcium oxychloride formation temperature increases as the initial salt concentration increases. The liquidus and eutectic temperature differ depending on both the initial salt concentration and the $Ca(OH)_2$:$CaCl$ molar ratio.
- At room temperature (23 °C), calcium oxychloride will form if the $CaCl_2$ concentration of the solution exceeds about 11.3 %. Further, the reaction between portlandite and $CaCl_2$ solution is fast (<15 min).
- Exposure of mortar samples to high concentration $CaCl_2$ solutions (greater than 15 % by mass) at room temperature (23 °C) produced degradation in mortar due to the formation of oxychloride even with no thermal cycling. The formation of calcium oxychloride is destructive and can cause damage and cracking.
- The core of the mortar specimens exposed to vacuum saturation with a solution of $CaCl_2$ concentration greater than 15 % remained unsaturated. X-ray fluorescence examination of these specimens also showed relatively no chloride ion ingress into the core of these samples. For these samples (samples with a $CaCl_2$ concentration greater than 15 %), it was

found that the majority of the porosity near the surface of the specimen is filled by the formation of solid calcium oxychloride, thereby filling/blocking the concrete pores and limiting further solution ingress.

- Mortar specimens exposed to concentrations greater than 15 % showed damage before freeze-thaw testing when the samples were immersed in the solution. For concentrations lower than 15 %, a reduction in dynamic elastic modulus was observed after one freeze-thaw cycle; in this range of concentration, mortar samples saturated with 8 % $CaCl_2$ solution showed higher freeze-thaw damage than a sample saturated with water which may correspond to a pessimism $CaCl_2$ salt concentration. However, the change in dynamic elastic modulus after one freeze-thaw cycle was not considerable for specimens saturated with concentrations greater than 15 %. This may be due to the fact that at concentrations greater than 15 %: 1) a large portion of solution in concrete pores is consumed by calcium oxychloride formation, and 2) the core of sample remained dry, which can provide enough space for ice formation.

5.0 Acknowledgements

6.0 References

[1]   W. Jones, Y. Farnam, P. Imbrock, J. Sprio, C. Villani, J. Olek, et al., An Overview of Joint Deterioration in Concrete Pavement: Mechanisms, Solution Properties, and Sealers, 2013. doi:10.5703/1288284315339.

[2]   W. Li, M. Pour-Ghaz, J. Castro, J. Weiss, Water absorption and critical degree of saturation relating to freeze-thaw damage in concrete pavement joints, J. Mater. Civ. Eng. 24 (2012) 299–307. doi:10.1061/(ASCE)MT.1943-5533.0000383.

[3]   Y. Qian, Y. Farnam, J. Weiss, Using Acoustic Emission to Quantify Freeze–Thaw Damage of Mortar Saturated with NaCl Solutions, in: Proc. 4th Int. Conf. Durab. Concr. Struct., Purdue University Libraries Scholarly Publishing Services, 2014: pp. 32–37. doi:10.5703/1288284315379.

[4]   Y. Farnam, D. Bentz, A. Sakulich, D. Flynn, J. Weiss, Measuring Freeze and Thaw Damage in Mortars Containing Deicing Salt Using a Low-Temperature Longitudinal Guarded Comparative Calorimeter and Acoustic Emission, Adv. Civ. Eng. Mater. 3 (2014) 316–337. doi:10.1520/ACEM20130095.

[5]   T.C. Powers, The air requirement of frost-resistant concrete, Highw. Res. Board. 29 (1949) 184–211. http://trid.trb.org/view.aspx?id=101611.

[6]   T. Powers, A working hypothesis for further studies of frost resistance of concrete, in: J. Am. Concr. Inst., Portland Cement Association, Detroit, Michigan, 1945: pp. 245–272. http://www.concrete.org/PUBS/JOURNALS/OLJDetails.asp?Home=JP&ID=8684 (accessed March 15, 2013).

[7]   P.K. Mehta, P.J. Monteiro, Concrete: microstructure, properties, and materials, Third, McGraw-Hill, New York, 2005.

[8]   S. Jacobsen, D. Sœther, E. Sellevold, Frost testing of high strength concrete: Frost/salt scaling at different cooling rates, Mater. Struct. 30 (1997) 33–42. http://link.springer.com/article/10.1007/BF02498738 (accessed April 09, 2013).

[9]   J.J. Valenza, G.W. Scherer, Mechanisms of salt scaling, Mater. Struct. 38 (2005) 479–488. doi:10.1007/BF02482144.

[10]   J. Marchand, E.J. Sellevold, M. Pigeon, The Deicer Salt Scaling Deterioration of Concrete - An Overview, in: V.M. Malhotra (Ed.), Third Int. Conf. Durab. Concr., Nice, France., 1994: pp. 1–46.

[11]   N. Ghafoori, R.P. Mathis, Scaling Resistance of Concrete Paving Block Surface Exposed to Deicing Chemicals, ACI Mater. J. 94 (1997) 32–38.

[12]   G. Scherer, Crystallization in pores, Cem. Concr. Res. 29 (1999) 1347–1358. doi:http://dx.doi.org/10.1016/S0008-8846(99)00002-2.

[13]   J. Kaufmann, Experimental identification of damage mechanisms in cementitious porous materials on phase transition of pore solution under deicing salt attack, École polytechnique fédérale de Lausanne (EPFL), 2000. http://library.eawag-empa.ch/empa_berichte/EMPA_Bericht_248.pdf (accessed March 15, 2013).

[14]   E.M. WINKLER, P.C. SINGER, Crystallization Pressure of Salts in Stone and Concrete, Bull. Geol. Soc. Am. 83 (1972) 3509–3514. doi:10.1130/0016-7606(1972)83[3509:CPOSIS]2.0.CO;2.

[15]   Z. Wang, Q. Zeng, L. Wang, Y. Yao, K. Li, Corrosion of rebar in concrete under cyclic freeze–thaw and Chloride salt action, Constr. Build. Mater. 53 (2014) 40–47. doi:10.1016/j.conbuildmat.2013.11.063.

[16]   R.W. Muethel, Investigation of Calcium Hydroxide Depletion as a Cause of Concrete Pavement Deterioration, 1997.

[17]   Y. Farnam, D. Bentz, A. Hampton, J. Weiss, Acoustic Emission and Low Temperature Calorimetry Study of Freeze and Thaw Behavior in Cementitious Materials Exposed to Sodium Chloride Salt, Transp. Res. Rec. 2441 (2014) 81–90.

[18]   M. Collepardi, L. Coppola, C. Pistolesi, Durability of concrete structures exposed to CaCl2 based deicing salts, in: V.M. Malhotra (Ed.), Durab. Concr. ACI SP-145, 3rd CANMET/ACI Int. Conf., 1994: pp. 107–120.

[19]   M. Pigeon, M. Regourd, The effects of freeze-thaw cycles on the microstructure of hydration products, Durab. Build. Mater. 4 (1986) 1–19.

[20]   X. Shi, L. Fay, M.M. Peterson, Z. Yang, Freeze–thaw damage and chemical change of a portland cement concrete in the presence of diluted deicers, Mater. Struct. 43 (2010) 933–946. doi:10.1617/s11527-009-9557-0.

[21]   L. Sutter, K. Peterson, S. Touton, T. Van Dam, D. Johnston, Petrographic evidence of calcium oxychloride formation in mortars exposed to magnesium chloride solution, Cem. Concr. Res. 36 (2006) 1533–1541. doi:10.1016/j.cemconres.2006.05.022.

[22]   L. Sutter, K. Peterson, G. Julio-Betancourt, D. Hooton, T.V. Dam, K. Smith, The deleterious chemical effects of concentrated deicing solutions on Portland cement concrete, Final Report for the South Dakota Department of Transportation, 2008.

[23]   A. Mesbah, M. François, C. Cau-dit-Coumes, F. Frizon, Y. Filinchuk, F. Leroux, et al., Crystal structure of Kuzel's salt 3CaO·Al2O3·1/2CaSO4·1/2CaCl2·11H2O determined by synchrotron powder diffraction, Cem. Concr. Res. 41 (2011) 504–509. doi:10.1016/j.cemconres.2011.01.015.

[24]   Y. Farnam, T. Washington, J. Weiss, The Influence of Calcium Chloride Salt Solution on the Transport Properties of Cementitious Materials, J. Adv. Civ. Eng. Hindawi. 2015 (2015) 1–13. doi:10.1155/2015/929864.

[25] K. Peterson, G. Julio-Betancourt, L. Sutter, R.D. Hooton, D. Johnston, Observations of chloride ingress and calcium oxychloride formation in laboratory concrete and mortar at 5°C, Cem. Concr. Res. 45 (2013) 79–90. doi:10.1016/j.cemconres.2013.01.001.

[26] P. Brown, J. Bothe, The system CaO-Al2O3-CaCl2-H2O at 23±2 °C and the mechanisms of chloride binding in concrete, Cem. Concr. Res. 34 (2004) 1549–1553. doi:10.1016/j.cemconres.2004.03.011.

[27] Y. Bu, D. Luo, J. Weiss, Comparing Fick's Second Law and the Nernst-Planck Approach in the Prediction of Chloride Ingress in Concrete Materials, Under Rev. (2014).

[28] A.K. Suryavanshi, J.D. Scantlebury, S.B. Lyon, Mechanism of Friedel's salt formation in cements rich in tri-calcium aluminate, Cem. Concr. Res. 26 (1996) 717–727. doi:10.1016/S0008-8846(96)85009-5.

[29] Y. Farnam, A. Wiese, D. Bentz, J. Davis, J. Weiss, Damage Development in Cementitious Materials Exposed to Magnesium Chloride Deicing Salt (In Press), Constr. Build. Mater. (2015).

[30] G.A. Julio-Betancourt, Effect of De-icers and Anti-icer Chemicals on the Durability, Microstructure, and Properties of Cement-based Materials, University of Toronto, 2009.

[31] C. Villani, Y. Farnam, T. Washington, J. Jain, J. Weiss, Performance of Conventional Portland Cement and Calcium Silicate Based Carbonated Cementitious Systems During Freezing and Thawing in the presence of Calcium Chloride Deicing Salts (In Press), Transp. Res. Board. (2015).

[32] C. Shi, Formation and stability of 3CaO·CaCl2·12H2O, Cem. Concr. Res. 31 (2001) 1373–1375. doi:10.1016/S0008-8846(01)00576-2.

[33] S. Chatterji, Mechanism of the CaCl2 attack on portland cement concrete, Cem. Concr. Res. 8 (1978) 461–467. doi:10.1016/0008-8846(78)90026-1.

[34] L. Berntsson, S. Chandra, Damage of concrete sleepers by calcium chloride, Cem. Concr. Res. 12 (1982) 87–92. doi:10.1016/0008-8846(82)90102-8.

[35] I.I. Vol'nov, E.I. Latysheva, Separation of calcium chloride from Solvay spent liquor through calcium hydroxichloride, J. Appl. Chem. U.S.S.R. 30 (1957) 1039–1046.

[36] S.Z. Makarov, I.I. Vol'nov, Figure 2061-System Ca(OH)2-CaCl2-H2O, in: C. Robbins (Ed.), Phase Diagrams Ceram. (Vol. 1), American Ceramic Society, Westerville, OH, 1964: p. 567.

[37] ASTM, ASTM C305 - Standard practice for mechanical mixing of hydraulic cement pastes and mortars of plastic consistency, in: ASTM International, West Conshohocken, PA, 2012. doi:10.1520/C0305-12.

[38] ASTM, ASTM C642 - Standard Test Method for Density, Absorption, and Voids in Hardened Concrete, in: ASTM, ASTM International, West Conshohocken, PA, 2013.

[39] D.P. Bentz, A virtual rapid chloride permeability test, Cem. Concr. Compos. 29 (2007) 723–731. doi:10.1016/j.cemconcomp.2007.06.006.

[40] Y. Farnam, H. Todak, R. Spragg, J. Weiss, Electrical Response of Mortar with Different Degrees of Saturation and Deicing Salt Solutions during Freezing and Thawing, Cem. Concr. Compos. 59 (2015) 49–59. doi:10.1016/j.cemconcomp.2015.03.003.

[41] Y. Farnam, M.R. Geiker, D. Bentz, J. Weiss, Acoustic Emission Waveform Characterization of Crack Origin and Mode in Fractured and ASR Damaged Concrete, Cem. Concr. Compos. 60 (2015) 135–145. doi:10.1016/j.cemconcomp.2015.04.008.

[42] ASTM, ASTM C597- Standard test method for pulse velocity through concrete, in: ASTM International, West Conshohocken, PA, 2009.

[43] J.M. Davis, D.E. Newbury, P. rao Rangaraju, S. Soundrapanian, C. Giebson, Milli X-ray fluorescence X-ray spectrum imaging for measuring potassium ion intrusion into concrete

samples, Cem. Concr. Compos. 31 (2009) 171–175.
doi:10.1016/j.cemconcomp.2008.12.005.

[44]   P.G. Debenedetti, H.E. Stanley, Supercooled and glassy water, Phys. Today. 56 (2003) 40–46. doi:http://dx.doi.org/10.1063/1.1595053.

[45]   C. Villani, R. Spragg, M. Pour-Ghaz, W. Jason Weiss, The Influence of Pore Solutions Properties on Drying in Cementitious Materials, J. Am. Ceram. Soc. 97 (2014) 386–393. doi:10.1111/jace.12604.

[46]   T.C. Powers, The physical structure and engineering properties of concrete, Res. Dep. Bull. Portl. Cem. Assoc. 90 (1958) 27 pages.

[47]   C. Abate, B.E. Scheetz, Aqueous Phase Equilibria in the System CaO-Al2O3-CaCl2-H2O: The Significance and Stability of Friedel's Salt, J. Am. Ceram. Soc. 78 (1995) 939–944. doi:10.1111/j.1151-2916.1995.tb08418.x.

[48]   D.R. Askeland, P.P. Fulay, W.J. Wright, The Science and Engineering of Materials, Cengage Learning, 2010.

[49]   T.C. Hansen, Physical structure of hardened cement paste. A classical approach, Mater. Struct. 19 (1986) 423–436. doi:10.1007/BF02472146.

[50]   T. Kim, J. Olek, Effects of Sample Preparation and Interpretation of Thermogravimetric Curves on Calcium Hydroxide in Hydrated Pastes and Mortars, Transp. Res. Rec. J. Transp. Res. Board. 2290 (2012) 10–18. doi:10.3141/2290-02.